UNIVERSITÄTSKLINIKUM HAMBURG-EPPENDORF

Klinik und Poliklinik für Neurologie

Prof. Dr. Tim Magnus

Generation and characterization of nanobodies against the ecto-enzymes CD39/CD73

Dissertation

zur Erlangung des Grades eines Doktors der Medizin an der Medizinischen Fakultät, der Universität Hamburg

vorgelegt von

Yinghui Duan

aus Henan (China)

Hamburg, August 2021

(wird von der Medizinischen Fakultät ausgefüllt)

Angenommen von der
Medizinischen Fakultät der Universität Hamburg am: 11.10.2021

Veröffentlicht mit Genehmigung der
Medizinischen Fakultät der Universität Hamburg.

Prüfungsausschuss, der/die Vorsitzende: Prof. Dr. Hans-Willi Mittrücker

Prüfungsausschuss, zweite/r Gutachter/in: Prof. Dr. Tim Magnus

Contents

1 Introduction

1.1 Extracellular purinergic signaling

1.1.1 ATP release to extracellular space

Intracellular nucleotides play a key role in the cell metabolism. When released to extracellular space, however, they can act as damage associated molecular pattern (DAMPs) and foster an inflammatory response (Bours et al. 2006). The nucleotide most well-known for its modulatory role in inflammation is adenosine triphosphate (ATP). In principal, ATP is stored intracellularly and acts as energy supplier for universal biological reaction, and intracellular ATP concentration is thousands times higher than that in extracellular space (1-10mM vs 20-100nM) (Forrester 1972). Since Geoffrey Burnstock found that ATP can act as extracellular neurotransmitter (Burnstock 1972), extracellular ATP has been widely studied and it has become clear that it is also an important mediator of inflammation. Extracellular ATP can be converted to adenosine diphosphate (ADP) and adenosine monophosphate (AMP) by the ecto-enzmye CD39 and AMP can be further converted to adenosine by the ecto-nucleotidase CD73. ATP can act as proinflammatory mediator by binding to receptors of the P2X family, especially to P2X7. In contrast, adenosine conducts anti-inflammatory signals by binding to receptors of the P1 family, such as ADORA2a.

Under certain conditions, such as inflammation, ischemia, hypoxia, necrosis and apoptosis, ATP is released from intracellular space to extracellular milieu and acting as DAMP. The release of ATP can occur via different mechanisms: cellular necrosis results in ATP egress from intracellular stores. Apoptotic cells, in contrast, release ATP through pannexin channels. During inflammation, pannexin and connexin channels are the main pathway to release ATP from vital cells (Eltzschig et al. 2012) (Idzko et al. 2014). If extracellular ATP level increase, interactions between ATP and purinergic P2 receptors are activated and downstream signaling cascades are triggered.

1.1.2 P2 purinergic receptors signaling

Purinergic P2 receptors are expressed on most immune cells, and according to their

chemical properties they are subdivided into two different subforms: metabotropic P2Y receptors (P2YRs) and ionotropic P2X receptors (P2XRs).

Metabotropic P2YRs belong to the large family of G-protein-coupled receptors (GPCR). P2YRs members bind ATP, ADP, uridine triphosphate (UTP), uridine diphosphate (UDP) and UDP-glucose to induce inflammation associated reactions. To date, eight subtypes of P2YRs have been identified: P2Y1R (ATP/ADP), P2Y2R (ATP/UTP), P2Y4R (UTP), P2Y6R (UDP), P2Y11R (ATP), P2Y12R (ADP), P2Y13R (ADP), and P2Y14R (UDP-glucose) (Jacobson et al. 2012) (Falzoni Simonetta et al. 2013) (Burnstock 2018). Except that P2Y11R was only identified and characterized in human, all the other P2YRs were cloned and characterized from mouse and human (Burnstock 2018).

Among all P2YRs that can bind ATP, P2Y2R is the critical receptor involved in inflammatory processes. Chen et al. found that the activation of P2Y2R on neutrophils plays an important role in controlling orientation and directing the migration of neutrophils (Chen et al. 2006). P2Y2R contributes to the development of graft-versus-host disease (GvHD), when compared to WT mice, serum IL-6 is decreased and CCL5, CCL22 and MMP9 in small intestine are downregulated in $P2Y2R^{-/-}$ mice (Klämbt et al. 2015). This study also showed that P2Y2R facilitates monocyte migration to inflamed GvHD target tissues. In idiopathic pulmonary fibrosis (IPF) patients, P2Y2R are functionally upregulated on macrophages and neutrophils and promote their migration and recruitment to lesion site (Müller et al. 2017).

For P2XRs, seven subtypes (P2X1-P2X7) are identified (Ralevic and Burnstock 1998), and they locate on cell membrane with a long loop exposed extracellularly, which constitutes the binding site for their ligands. In contrast to P2YRs, P2XRs are all activated by extracellular ATP. P2XRs have a trimeric structure and can bind to three ATP molecules simultaneously, which triggers the open of ion channels for Na^+ and Ca^{2+} influx and K^+ efflux (Idzko et al. 2014). All P2XRs have been shown to participate in some ways in inflammatory reactions, however, P2X7 is probably the most investigated P2X7 receptor in the context of inflammation, due to its role in inflammasome activation and its involvement in a variety of inflammation-related diseases, including cancer and infectious diseases (Savio et al. 2018). Shieh and

colleagues stimulated the cultured mouse primary macroglia (WT and P2X7$^{-/-}$) with ATP, they found that P2X7 activation evokes the release of pro-inflammatory factors, such as interleukin 6 (IL-6), tumor necrosis factor (TNF) and C-C motif chemokine ligand 2 (CCL2) (Shieh et al. 2014). P2X7 is also proved to play a crucial role in a variety of inflammation related intracellular pathways, such as NOD-, LRR- and pyrin domain-containing protein 3 (NLRP3), nuclear factor kappa-light-chain-enhancer of activated B cells (NF-kB) and vascular endothelial growth factor (VEGF) (Di Virgilio et al. 2017) (Adinolfi et al. 2018) .

Both P2Y2R and P2X7R activations are double-edge swords. On the one hand, when activated properly, they are pro-inflammatory and corresponding immunological responses can facilitate elimination of cancer cells or invading pathogens. On the other hand, activation of these receptors can also contribute to chronic inflammatory diseases progression, such as asthma, COPD (chronic obstructive pulmonary disease) and IBD (inflammatory bowel disease) (Lommatzsch et al. 2010) (Figliuolo et al. 2017), which will prolong the course of disease and impact prognosis.

1.1.3 Molecular biology and function of CD39 and CD73

The level of extracellular nucleotides are mainly regulated by a system of ecto-enzymes consisting of several families, including ecto-nucleoside triphosphate diphosphohydrolases (ENTPDases), ecto-5'-nucleotidase (CD73), ecto-nucleotide pyrophosphate phosphodiesterases (ENPPs) and NADase (CD38). Among NTPDases, four subtypes (ENTPDase-1, 2, 3 and 8) are transmembrane proteins and ENPDase-1 (CD39) is seen as the prototype of this family (Knowles 2011). CD39 can convert ATP or ADP to AMP, which can be further degraded to adenosine by CD73. Therefore, CD39 and CD73 form a two-step pathway in converting ATP to adenosine (**Figure 1**).

CD39 is fixated on the membrane via two trans-membrane domains, with N- and C-terminus in cytoplasm for signaling and a long loop for substrate binding in extracellular space. The extracellular loop consists of five apyrase conserved regions (ACRs) and is responsible for ATP binding and degradation (Robson et al. 2006). CD73 is a glycosyl-phosphatidyl inositol (GPI)-anchor protein on the cell membrane and functions as homodimer in converting AMP to adenosine.

CD39 and CD73 are expressed on immune cells, such as B cell, T cell, neutrophils,

endothelial cells and dendritic cells. Besides, they are also upregulated on several tumor cells (reviewed in (Allard et al. 2016)). It is worth mentioning that there are species specific differences in the expression pattern of CD39 and CD73 on immune cells: murine regulatory T (Treg) cells show high expression of both CD39 and CD73. In contrast, human Treg cells express CD39 on cell surface, while CD73 is expressed predominately in the cytoplasm. Expression of these two ecto-nucleotidases varies during CD8+ T cell differentiation, where CD39 and CD73 are upregulated and downregulated respectively (Bono et al. 2015).

1.1.4 P1 purinergic receptors signaling

Once generated in the extracellular milieu, adenosine binds to and activates purinergic P1 receptors (Falzoni Simonetta et al. 2013). As P2YRs, P1 receptors are GPCRs and are defined as four subtypes: A1R, A2AR, A2BR and A3R (Jacobson et al. 2012). According to the effect on adenylyl cyclase (AC) activity regulation after activation, receptors are functionally characterized as two groups: A1R and A3R are preferentially coupled to Gi/o protein and inhibit AC activity and cyclic AMP (cAMP) production, while A2AR and A2BR are coupled to Gs protein and promote AC in intracellular cAMP generation (Borea et al. 2015). P1Rs are express in many tissues, however, A2AR and A2BR are mainly involved in inflammation associated responses and mediate anti-inflammatory effect (Eckle et al. 2009) (Chen et al. 2013) (Haskó and Cronstein 2013). Further, it has been shown that A3R induces neutrophils migration and recruitment (Chen et al. 2006).

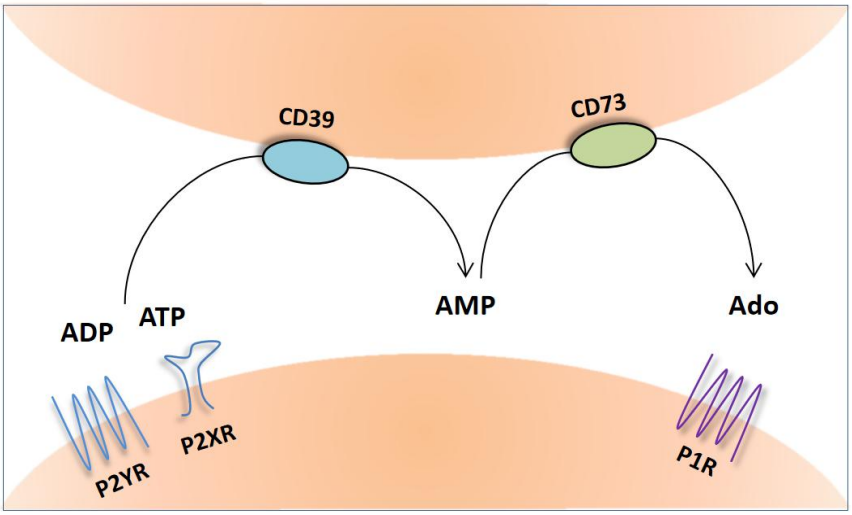

Figure 1: CD39/CD73-dependent ATP degradation pathway and receptors. Extracellular ATP and ADP are hydrolyzed by CD39 to AMP and subsequently CD73 dephosphorylates AMP to adenosine. Receptors for extracellular nucleotides comprise three families, the metabotropic P1 and P2Y receptors (P2YR) and ionotropic P2X receptors (P2XR). P1 receptors are activated by adenosine, P2YR by various metabolites of ATP and UTP, and P2XR by ATP.

1.2 Antibodies

The bodies defense against invading pathogens, comprises two distinct types of immune responses, a fast innate immune response and specialized adaptive immune response. The former occurs rapidly after the infection and is the first defense line in destroying microorganisms. However, only microorganisms with common pathogenic structures are detected and eliminated. To ensure protection over a longer period of time, the adaptive immune system generates antigen-specific lymphocytes. Although an adaptive immune response takes longer to develop, the benefit is in its high specificity towards the pathogen and the development of long living memory cells that prevent reinfection with the same pathogen by ensuring rapid pathogen elimination. The two pillars of adaptive immune response are T cell-mediated responses to remove intracellular pathogens and B cell-generated antibodies to eliminate pathogens in extracellular space.

1.2.1 Conventional antibody

Since von Behring and Kitasato first reported the existence of specific agents against diphtheria toxin in serum (von Behring and Kitasato 1890), antibodies, also known as immunoglobulins, have been discovered and explored for more than 100 years. An

antibody is a “Y”-shaped protein that is secreted by plasma cells that develop from B cells. Antibodies are essential for the neutralization of virus to prevent infection of host cells and for the opsonization of bacteria to mark them for phagocytosis.

Antibody consists of two identical heavy chains (H) and two identical light chains (L) which are connected by disulfide bonds. H and L both can be separated into antigen binding variable domains (V) and specify effector functional constant domains (C) (**Figure 2**). Due to the difference of C domains of H-chain, antibodies are divided into five isotypes, defined as IgA, IgD, IgE, IgG, and IgM. Among five isotypes, IgG is the main functional soluble antibody in circulation which accounts for approximately 70-75%. Herein, we mainly focus on the structure and function of IgG, and antibody hereafter refers to IgG.

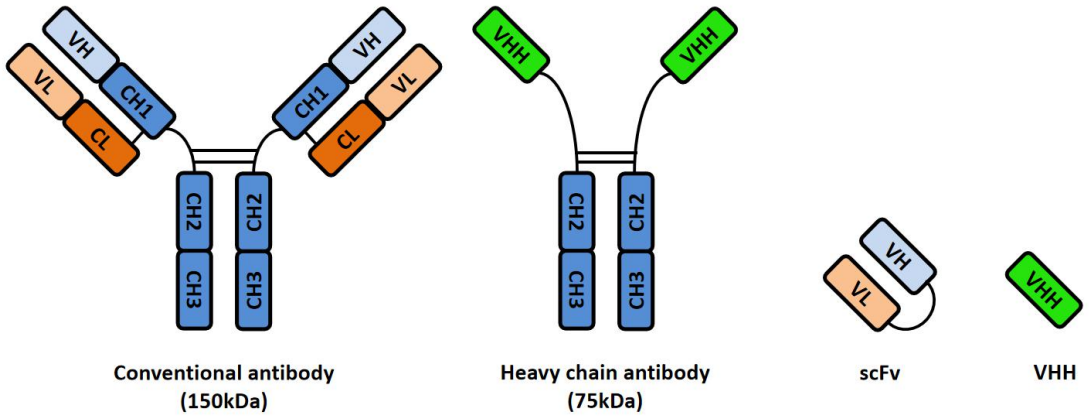

Figure 2: Schematic representation of conventional antibody and heavy chain antibody. Conventional antibody comprises of two identical light chains and two identical heavy chains. The variable domain of VH and VL form the functional antigen-binding fragment, and scFc is the smallest fragment of conventional antibody with antigen-binding specificity. HcAb lack light chains and as well as the constant domain CH1. The single variable domain of the HcAb can specifically bind to antigens.

For an antibody, H-chain consists of four domains (one V domain (VH) and three C domains (CH1, CH2 and CH3)), whereas the L-chain only has 2 domains (one V domain (VL) and one C domain (CL)) (**Figure 2**). Antibodies can be separated into two different regions: the Fab (antigen-binding fragment) region resembles one arm of Y shape antibody consisting of the L-chain, as well as the VH and CH1 domain of H chain. The Fab fragment contains the antigen binding paratope, which is highly variable. One the other side, antibodies have an Fc fragment that contains CH2 and CH3 domains of two heavy chains. This Fc fragment is used to define IgG sublasses

and its function is in the interaction with Fc receptors on immune cells or the activation of the complement system (Schroeder and Cavacini 2010).

1.2.2 Heavy chain antibody

In 1993, Hamers and colleagues first described a new naturally occurring antibody in camelids, which they termed heavy-chain antibodies (Hamers-Casterman et al. 1993). In the next few years, heavy-chain antibodies (HCAb) were also found in nurse shark, where it was named immunoglobulin new antigen receptor (Ig-NAR) (Greenberg et al. 1995). The structure of HCAbs is strikingly different from conventional antibody (**Figure 2**). HCAb lack the light chain and are devoid of the CH1 domain of the heavy chain. However, its variable domain of the heavy chain (VHH) can recognize specific antigens without assistance of other domains, which makes VHH the smallest functional and available intact antigen binding fragment derived from an antibody. Inspired by and based on its antigen-binding capacity and small size, Cortez-Retamozo and colleagues first termed this entity as nanobody (Nb) (Cortez-Retamozo et al. 2004).

1.2.3 Structural differences between VH and VHH

VH of conventional antibodies and VHH of HCAbs exhibit striking genetic and structural differences (**Figure 3**). Genetically, VH and VHH exhibit homologous regions, both contain four framework regions (FRs) and three complementary determining regions (CDRs). Muyldermans first demonstrated that four remarkable amino acid substitutions occur in the FR2 in VHH (Muyldermans et al. 1994), which mark important interaction regions of VH and VL in the VH domain. Thus, these substitutions grant the VHH domain a more hydrophilic character (Muyldermans et al. 1994) (Vu et al. 1997). Except difference in the conserved FR regions, as shown in **Figure 3**, VHH harbor longer hypervariable regions than VH on average. The length of CDR1 and CDR2 are relatively limited, while the sequence of CDR3 is extended. The CDR3 of VHHs shows a greater sequence diversity than of VHs, and this is mainly achieved by incorporating of three to four additional residues (Mitchell and Colwell 2018b). The prolonged CDR1, CDR2 and CDR3 comprise a convex antigen-interacting surface. The CDR3 is the dominate loop in determining nanobody specificity and facilitates nanobodies to bind into cavities of its target, such as the

active site of enzymes (Desmyter et al. 1996) (Mitchell and Colwell 2018a). In general, a conserved disulfide bond connecting CDR1 and CDR3 is formed to restrict the VHH hypervariable domain flexibility in the absence of antigens (Muyldermans et al. 1994) (Govaert et al. 2012).

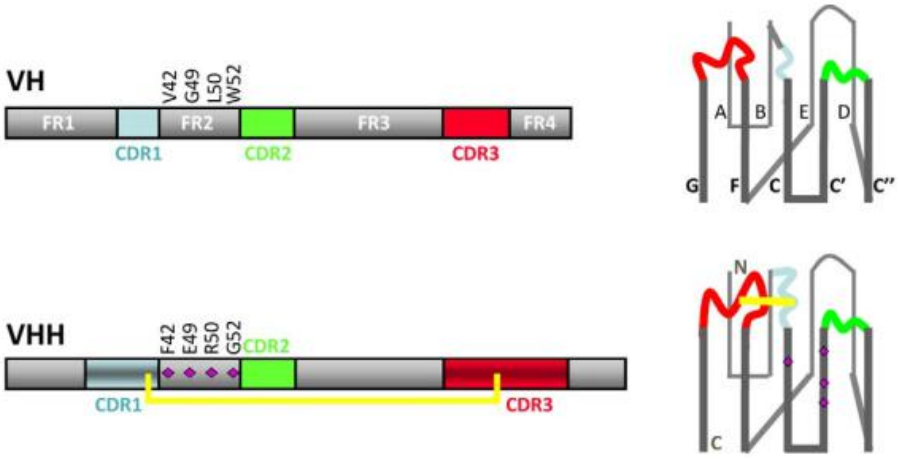

Figure 3: Schematic of VH and VHH sequences and scaffold structures. Both VH and VHH contain four framework regions (FRs) and three complementary determining regions (CDRs). In VHH FR2, four residues are replaced by hydrophilic amino acids (V42F, G49E, L50R and W52G). CDRs lengths are extended in VHHs, especially CDR3, and CDR1 is linked to CDR3 with a sulfide bond (left). VH and VHH are architected with 9 β-stranded sheets. The CDRs prolate and form the antigen-binding surface, which is relatively plain in the VH, while the enlarged CDR3 of the VHH allows the formation of a convex paratope. Replacement of residues in VHH FR2 are exposed to solvent that contributes to the solubility of nanobody (right). Adopted from (Flajnik et al. 2011)

Due to substitutions from hydrophobic residues to hydrophilic residues in FR2 and disulfide bond connecting CDR1 and CDR3 in scaffold structure described above, when compared with cAb, nanobody is more soluble, more stable, and devoid of aggregation (Hussack et al. 2011). Nanobody exhibits a high affinity to their antigens and retain 80-100% activity after incubated at 37℃ for 200h, making them suitable for *in vivo* applications (Ghahroudi et al. 1997). Goldman et al. summarized several methods to enhance nanobody stability, which can contribute to the application of nanobody *in vivo* (Goldman et al. 2017).

With only 15kDa in size, nanobody is one-tenth the size of conventional antibody (150kDa), and half the size of smallest intact antigen-binding fragment (scFv) derived from conventional antibody. The small size enables nanobody to exhibit thorough tissue penetration, and some nanobody exhibited the ability to cross the blood brain barrier, where remains challenge for diagnosis and therapy (Jank et al. 2019). On the

other hand, due to their small size, nanobody has a fast pharmacokinetics and are excreted rapidly via the kidneys after administration. To extend the half-life of nanobody *in vivo*, several modifications can be made, such as generating homo-dimeric nanobodies, hetero-trimeric nanobodies containing one anti-albumin nanobody nanobody, and IgG-Fc fusion proteins (Wesolowski et al. 2009). When compared with cAb, nanobody lacks the Fc domains and shares a relatively high identical sequence of human VH, thus it exhibits a low immunogenicity (Ackaert et al. 2021).

1.3 Phage display

1.3.1 Filamentous phage

The common bacteriophage has a head and a tail and injects its linear genome into the host cytoplasm, where it can replicate and assemble new phages to generate its progeny. Ultimately, the bacterial host is destroyed to release newly produced virions. However, also other bacteriophages with a different morphology and lifecycle exist. One of them is filamentous bacteriophage. Among the filamentous bacteriophage, F pilus-specific phage (f1, M13 and fd) are the best-known, and are also widely used in phage display technique. It is widespread among Gram-negative bacteria, and Escherichia coli bacteria are the most common host (Mai-Prochnow et al. 2015).

The filamentous bacteriophage comprises of a long thin filamentous tube containing a circular single-stranded DNA. The genome consists of only nine genes, but eleven proteins are encoded (Rakonjac et al. 2011). Among all proteins, pIII and pVIII are important coat proteins in building the filamentous morphology, as well as in phage display process where they provide the platforms to display foreign peptides. The major coat protein pVIII, which contains up to 2700 copies, is the critical components of the filamentous tube. The minor coat protein pIII (five copies only) is mainly assembled on the tail, and plays a key role in mediating bacteria infection through interacting with F-pilus (Kehoe and Kay 2005) (Rakonjac et al. 2011).

On contrast to the archetypal bacteriophage, the filamentous bacteriophage undergoes a non-lytic lifecycle. The single-stranded DNA is injected into the bacterial cytoplasm and acts as template, where double-stranded DNA is synthesized with the help of host enzymes. The replication of filamentous bacteriophage, known as rolling cycle

replication, is dramatically different from lytic cycle and will generate many single-stranded linear copies of original DNA which will be further converted to double-stranded circular DNA (Ruiz-Masó et al. 2015). The bacterial machinery facilitates phage particles generation, followed by assembling and extrusion from bacteria (Rakonjac et al. 2011). However, if a phagemid vector is used for infection, a helper phage will be necessary to package, assemble and release the phages (Kehoe and Kay 2005).

1.3.2 Insertion of foreign genes into the phagemid genome

In 1985, Smith first introduced the possibility of inserting a foreign gene into a bacteriophage genome without interfering with its function. The result was that this phage displayed the expressed gene as part of the coat protein (Smith 1985). In past decades, this technology has been extensively studied and further developed, and the derived phage display technique is widely used in the generation of nanobody (McCafferty et al. 1990) (Clackson et al. 1991) (Winter et al. 1994) (Eden et al. 2018) .

Antigen-specific nanobodies usually are selected from a nanobody library. In order to generate a nanobody library, the first step usually is the immunization of camelids, such as llamas with a target protein or an expression plasmid encoding the target protein. After several rounds of boosting immunization, B cells are isolated from peripheral blood, mRNA is extracted subsequently, and cDNA is synthesized by reverse transcription. With the help of proper primers, VHH frameworks are amplified by PCR simultaneously introducing specific restriction sites which allow cloning into a phagemid vector. For this, the PCR products and vector are digested with specific restriction enzymes and ligated to generate phagemid library encoding the comprehensive VHH repertoire genes of the isolated B cells. The ligation products are used to transform bacteria and helper phages are used to produce a phage library that can display VHH domains on coat proteins. The phages can be precipitated by PEG and prepared for target protein specific VHH selection (**Figure 4**).

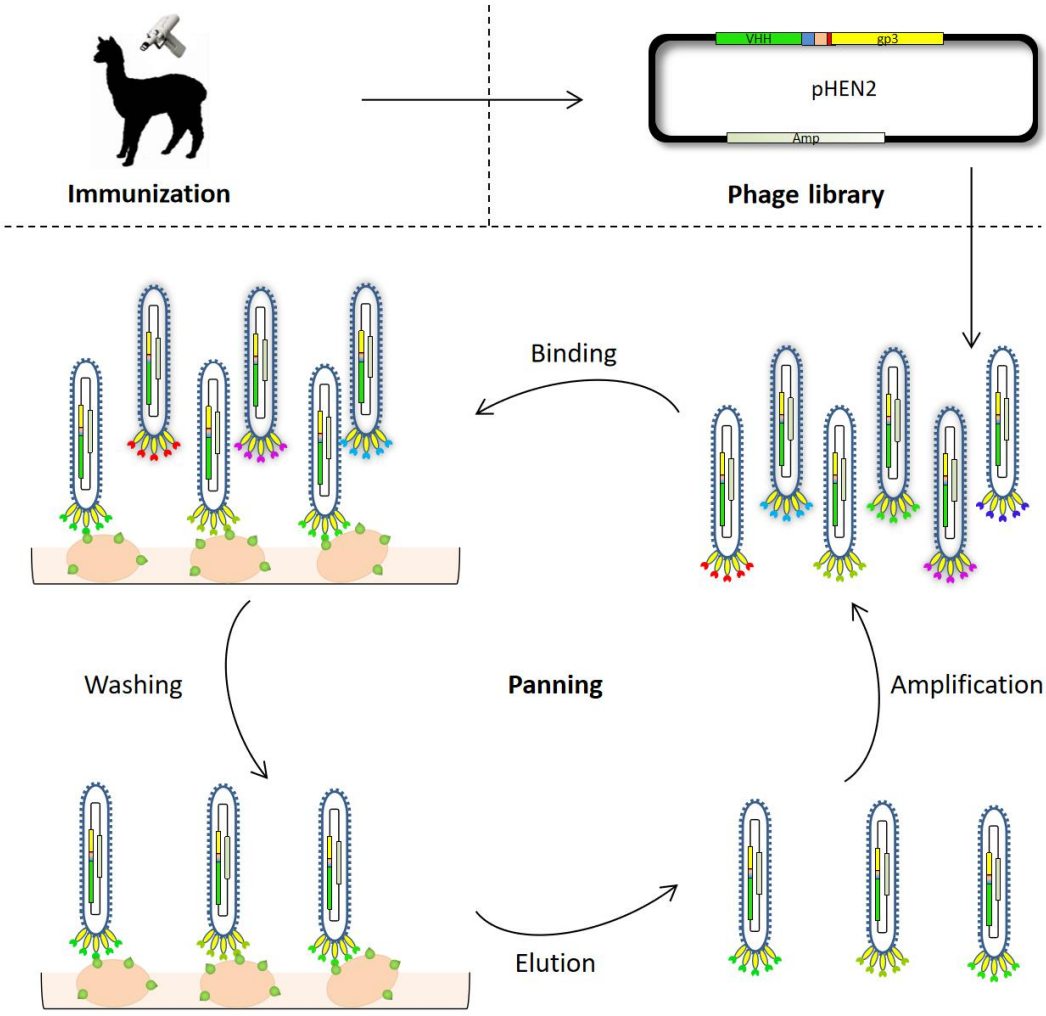

Figure 4: Phage display for the selection of antigen-specific nanobodies. Camelids can be immunized with plasmids encoding the target antigen. The VHH coding region is cloned into a phagemid. Via cloning into the phagemid, the VHH domain is genetically fused to the gp3 coat protein of the phage. Antigen-specific clones are enriched from the phage display library by panning on cells transfected with target antigen. Bound phages are eluted followed by another round of panning with the eluted phages.

1.3.3 Selection of antigen-specific nanobodies

McCafferty and colleagues challenged the traditional method of generating monoclonal antibody (mAb) by use of the hybridoma technology, when they displayed the variable domains of conventional antibody on the surface of bacteriophage and used antigen to select bacteriophage that expresses high antigen-specific variable domains (McCafferty et al. 1990). This creative and impressive technology was awarded the Nobel Prize in Chemistry on 2018 (2018).

This process is known as bio-panning (Parmley and Smith 1988), aiming to remove

non-target nanobodies and enrich antigen-specific nanobody clones. Bio-panning bases on the antigen-antibody specific interaction feature. Target antigens are immobilized on microtiter plate or expressed on the cell surface to provide available epitopes. The phage library is added and allowed to establish antigen-antibody binding, followed by the washing step which eliminates unbound phages. The phages that display antigen specific antibodies are eluted and multiplied. Helper phage assists the phage progeny in packing, assembly and extruding from the host. Through PEG precipitation, a new phage library with higher fraction of antigen binding nanobodies is generated. The bio-panning can be repeated several times in order to produce high specific antibodies. Further, washing conditions can also be adjusted in order to specifically enrich e.g. for high affinity binders.

In this thesis, the experimental focus is on the ATP degrading and adenosine-generating ecto enzymyes CD39 and CD73. The generation and further development of biologics or small chemical compounds which act as antagonists of CD39 or CD73 are of great general interest, especially since CD39 and CD73 play a role in the suppression of anti-tumor immune responses (Ghalamfarsa et al. 2019) (Allard et al. 2020). POM-1, a non-specific CD39 inhibitor, first showed anti-tumor proporties (Sun et al. 2010). mAbs against CD39 (such as BY40 and BA54G (Bonnefoy et al. 2015)) or CD73 (such as MEDI9447 (Overman et al. 2018)) have already been generated, demonstrating promising therapeutic potential as anti-tumor reagents. Nanobodies, compared with mAbs and chemical products, have the combinative advantages of specificity, low immunogenicity, enzyme catalytic site readiness, barrier penetration and tunable half-life. Therefore, the generation of CD39 and/or CD73 specific functional nanobodies seems to be the next logical step towards new effective anti-tumor reagents that aim at blocking the generation of immunosuppressive adenosine in order to improve the endogenous anti-tumor immune response.

2 Materials

2.1 Laboratory equipments

Equipment	Model	Company
Analytical scale	PL602-S	Mettler-Toledo
Cell chamber	Neubauer	Marienfeld-Superior
Centrifuge	5430 R	Eppendorf
	5810 R	Eppendorf
DNA Gel Electophoresis	Sub-Cell GT	BioRad
Flow Cytometer	FACSCelesta™ Flow Cytometer	BD Biosciences
	FACS Aria-IIIu Sorter	BD Biosciences
Freezer	-20°C	Liebherr
	-80°C	Panasonic
Fridge	4°C	Liebherr
High-performance liquid chromatography (HPLC)	1260 Infinity	Agilent Technologies
Incubator	MCO-5ACUV	Panasonic
Luminescent machine	Vector 2	Perkin Elmer
Microscope	Axiovert 40 CFL	ZEISS
Microwave		AEG
Multipette		Eppendorf
Nanodrop	Nanodrop 2000c	Thermo Scientific
OD600 DiluPhotometer		Implen
Polymerase chain reaction (PCR)	Nexus X2	Eppendorf
Pipetteboy		Integra
Protein Gel Electophoresis	Mini-Cell	Novex
Scanner	4990	Epson
Shaker incubator	Ecotron	INFORS HT
ThermoMixer	F1.5	Eppendorf
Ultraviolet transilluminator	TFL-35M	Vilber Lourmat
Vibration shaker	Roto-Shake Genie	Scientific Industries
Vortex	54113	Heidolph
Waterbath	GLS400	Grant
	1002	GFL
Workbench	Class II Type A/B3	Baker

2.2 Consumables

Material	Type	Company
Cell culture flasks	T25, T75	Greiner
96-well white plate		Nunc
96-well plate		Greiner
Combitips	various sizes	Eppendorf
FACS tubes		SARSTEDT
Falcon tube	15ml, 50ml	Greiner
Gloves	Coated	Ansell
	Nitra-Tex	Ansell
Microcentrifuge tubes	various sizes	Eppendorf
Parafilm	PM-996	Bemis
Pipette tips	various sizes	Eppendorf
	various sizes	Th.Geyer
Plates for bacteria		Greiner
SDS PAGE gel	4-12% NuPAGE	Invitrogen
Serological pipettes	various sizes	Greiner

2.3 Reagent (kits)

Purpose	Name	Company
PCR-purification	Nucleospin Extract II	Macherey-Nagel
Sequencing	Mix2Seq Kit	Eurofins
	PlateSeq Kit Mix OVERNIGHT	Eurofins
Plasmid purification	Miniprep Kit	Qiagen
	Endofree Maxiprep Kit	Qiagen
CD39 Functional Assay	CellTiter-Glo® Luminescent Cell Viability Assay Kit	Promega
CD73 Functional Assay	AMP-Glo™ assay Kit	Promega

2.4 Chemicals

Chemicals	Company
2YT Broth	Invitrogen
AEBSF	Merck
ATP	Sigma
Bacto agar	BD/Difco
Bacto tryptone	BD/Difco
Bovine serum albumin, BSA	Sigma
Carbenicillin	Gibco
Coomassie stain	Bio-Rad

DMEM medium	Gibco
dNTPs	Thermo Fisher Scientific
eAMP	AG Tolosa
EDTA	Sigma
FBS Good Forte	PAN seratech
FreeStyle™ 293 Expression Medium	Gibco
Glucose	Carl-Roth
Glycerol	Sigma
JetPEI	Polyplus
Kanamycin	Gibco
LB Agar	Invitrogen
LB Broth	Invitrogen
Loading Dye, 6×	Thermo Fisher Scientific
Magnesium chloride, MgCl2	Sigma
MES buffer, 20x	Invitrogen
NuPAGE antioxidant	Invitrogen
NuPAGE sample reducing agent, 10x	Invitrogen
NuPAGE SDS-PAGE sample buffer, 4x	Invitrogen
PBS, 1x	Gibco
Polyethylene glycol (PEG)	Merck
Pen/Strenp	Gibco
Potassium chloride, KCl	Merck
PSB-14685	AG Tolosa
Recombinant huCD73	AG Koch-Nolte
Roti-GelStain	Carl Roth
Sodium chloride, NaCl	Merck
TAE	Invitrogen
Trypsin, 1x	Gibco
UltraPure Agarose	Invitrogen

2.5 Mediums

	Composition
Bacterial culture medium	
2YT-Medium	32g/l in deionized Water
2YT-Agar	32g/l 2YT Broth in deionized Water
	15g/l Bacto agar in deionized Water
LB-Medium	20g/l in deionized Water
LB-Agar	32g/l in deionized Water
SOC-Medium	2%(w/v) Tryptone

	0.5%(w/v) Yeast extract
	10mM NaCl
	2.5mM KCl
	10mM $MgCl_2$
	20mM Glucose
Eukaryotic medium	
Complete DMEM	DMEM (1x) + GlutaMax
	10% FCS
	1% Pen/Strep
Feeding medium (for transfected HEK-6e cells)	FreeStyle™ 293 Expression Medium
	20% tryptone

2.6 Buffers

Buffer	**Composition**
Block buffer for bio-panning	DMEM (1x) + GlutaMax
	10%FCS
	1%BSA
FACS buffer	PBS
	0.2% BSA
	1mM EDTA
PEG/NaCl buffer	de-ionized H_2O
	20% PEG
	250 mM NaCl
SDS-PAGE gel running buffer (1x)	20x MES buffer diluted in de-ionized water

2.7 Antibodies

Antigen	**Fluorochrome**	**Clone**	**Company/Institute**
Human CD39	APC	A1	BioLegend
Mouse CD39	PE	24DMS1	Thermo Scientific
Human CD73	BV421	AD2	BioLegend
Mouse CD73	eFlour450	eBioTY/11.8	Thermo Scientific
	PE	TY/11.8	BioLegend
Rabbit IgG(H+L)	PE	None	Dianova
	APC	None	Dianova
Mouse CD4	BV421	L3T4	BioLegend
Mouse CD25	APC	PC61	BioLegend
Human CD8	BV421	RPAQT8	BioLegend

Human CD4	Alexa 488	RPAQT4	BioLegend
Human CD25	BV421	BC96	BioLegend
Human CD127	PerCP5.5	HCD127	BioLegend

2.8 Enzymes

Polymerase	**Company**
Taq Dream DNA Polymerase	Thermo Scientific

Restriction Enzymes	**Company**
EcoRI-HF	NEB
NotI/NotI-HF	NEB
NocI-HF	NEB
PciI	NEB

Ligase	**Company**
T4 Ligase	NEB

2.9 DNA- and protein standards

Standard	**Company**
GeneRule, 1kb plus DNA Ladder	Thermo Scientific
GeneRule, Low Range DNA Ladder	Thermo Scientific
PageRule™ Prestained Protein Ladder, 10 to 180 kDa	Thermo Scientific

2.10 Oligonucleotides (primers)

Name	**Sequence**
CMV forward	CGCAAATGGGCGGTAGGCGTG
LMB3	CAGGAAACAGCTATGAC
M13 forward	CAGGAAACAGCTATGAC
M13 reverse	GTAAAACGACGGCCAGT
TE155 (to introduce PciI restriction site)	GGTGACATGTCTCAGGTGCAGCTGGTGGAG TCTG
TE156 (to introduce NotI restriction site)	TGGTTGTGGTTTTGGTGTCGCGGCCGCTGAG GAGACGGTGACC
SHF	TCGCGGCCCAGCCGGCCATGGCGCAGGTSM ARCTGCAGGAGTCWGG
LHF	TCGCGGCCCAGCCGGCCATGGCCGATGTGC AGCTGCAGGMGTCWGGRGGAGG
IgG2b rev	AGGATTGGGTTGTGGTGCGGCCGCTGGTTGT GGTTTTGGTGTCTTGGGTTC

IgG2c_rev	CCTGGGCATTTGGGAGCGGCCGCGCTGGGG TCTTCGCTGTGGTG

2.11 Plasmids and phagemids

Gene of Interested	Vector
Entpd1 (Mouse CD39)	pCMV-Sport6
ENTPD1 (Human CD39)	pCMV-Sport6
Nt5e (Mouse CD73)	pCMV-Sport6
NT5E (Human CD73)	pCMV-Sport6
VHH repertoires	pHEN2
VHH repertoires	pCSE2.5-Rabbit Fc

2.12 Pro- and eukaryotic cells

Cells	Company or Institute
Prokaryotic cells	
XL-1 Blue competent cells	ATCC
TG1 competent cells	AG Koch-Nolte
Eukaryotic cells	
HEK 293-T	AG Magnus
HEK 293-6E	AG Koch-Nolte
Human PBMC (Donor: 19BC17)	AG Tolosa
Mouse spleen cells (Strain: C57BL/6)	AG Koch-Nolte

2.13 Helper phages

	Company
M13K07 helper phage	BioLab

2.14 Software

Program
FlowJo
Prism 5
SnapGene Viewer

3. Methods

3.1 Molecular biological methods

3.1.1 Quantification of DNA

The concentration of purified DNA (plasmids, Gel purified DNA fragments) was measured by Nanodrop spectrophotometry. The ratio of absorbances A260/A280 was used to evaluate the purity of DNA. When the ratio of DNA sample ranged from 1.8 to 2.0, samples were assessed to be sufficiently pure.

3.1.2 Reverse transcription (RT) and polymerase chain reaction (PCR)

RNA extraction from alpaca peripheral blood lymphocytes was done by EuroGentech as part of the immunization service. Reverse transcription to complementary DNA (cDNA) was completed by AG Koch-Nolte.

3.1.3 DNA-sequencing

The DNA-Sequencing tasks were all performed by Eurofins. For this, 750-1500ng plasmid DNA with 20pmol of corresponding primers were used. The evaluation was carried out with 4 peaks software.

3.1.4 Agarose gel electrophoresis and gel purification

DNA fragments were size fractionated by agarose gel electrophoresis and further purified. For this purpose, 1-2% agarose gels containing Roti-Gelstain were generated. Samples were prepared with appropriate volume of 6× loading buffer and loaded in wells of the gel. According to size of DNA fragments, gels were run at 120V for 40-45min. The DNA bands were visualized and documented with a UV transilluminator. DNA bands at correct size were excised from gels for further purification.

For gel purification, Nucleospin Extract II (Macherey-Nagel) kit was used, and DNA was purified according to manufacturer's protocol. Finally, DNA fragments were eluted with 20µl TE elution buffer or distilled water, which were further used for ligation.

3.1.5 Restriction enzyme digestion of DNA

Restriction digestion of double-stranded DNA was performed, and appropriate

restriction endonucleases and buffers from New England Biolabs (NEB) were used depending on the purpose and restriction site in the plasmid. The temperature for digestion and inactivation, as well as the buffer conditions for digestion were chosen according to manufacturer's recommendations. However, when digestion was performed with two enzymes, the optimized buffers and conditions were chosen according to the recommendation of NEB. The following enzyme combination, time and temperature were used for the restriction digestion:

Interested-DNA	Enzyme 1	Enzyme 2	Temperature	Duration
Ordered DNA/pCMV sport 6 target vector	EcoRI-HF	NotI-HF	37°C	2h
VHH-amplification/pHEN2 target vector	SfiI		50°C	16h
		NotI	37°C	2h
VHH-pHEN2 (without internal NcoI restriction site)/pCSE 2.5 target vector	NcoI-HF	NotI-HF	37°C	2h
VHH-pHEN2 (with internal NcoI restriction site)	PciI	NotI	37°C	2h

3.1.6 Ligation of DNA fragments

Before ligation, the digested interested DNA and vector were purified from agarose gel, as mentioned in **Section 3.1.4**. For the ligation reactions, T4 ligase and the ligation buffer from NEB were used. DNA fragments of interest and vector backbone were ligated in a molar ratio of 1:2 (insert : vector) in a 20µl reaction condition at 16°C overnight. As control, a ligation mixture containing only the vector backbone was used.

3.1.7 Transformation of competent bacteria

Chemically competent bacteria (XL1 blue E.coli) were transformed by heat shock. 50µl bacteria aliquot were taken directly from -80°C stocks and thawn on ice. Appropriate amounts of plasmid DNA or ligation products were added to bacteria and incubated on ice for 20-30 minutes. After the heat shock at 42°C for 45s, bacteria-DNA mixtures were put back on ice for another 2min and shaken at 37°C at 200 rpm after addition of pre-warmed 450µl SOC medium. Appropriate volume of incubated bacteria-DNA mixtures was plated on LB agar plates with appropriate antibiotics and incubated at 37°C overnight. An appropriate number of colonies was picked for plasmid purification.

3.1.8 Cultivation of bacteria

Bacteria were cultured in LB-Carb or 2xYT-Carb medium. For this purpose, individual colonies were picked from LB^{+Carb} or $2xYT^{+Carb}$ agar plates and cultivated in a suitable volume of corresponding medium (final concentration of carbenicillin: 100µg/ml). Pre-cultures were incubated at 37°C 200 rpm overnight.

3.1.9 Purification of plasmid DNA from bacteria

Single colonies were picked and cultivated in 5ml or 100ml LB^{+carb} medium for Mini-preparation or Maxi-preparation respectively. The plasmid purification was carried out according to the protocol of Spin Miniprep or Maxiprep kits (Qiagen).

3.1.10 Protein SDS-PAGE gel electrophoresis

In order to analyze the production efficiency of human embryonic kidney 6E (HEK-6E) cells transfected with nanobody expression plasmids, 6.5µl supernatant was mixed with reducing buffer and staining buffer, then the mixture was incubated at 70°C for 10min to denature the protein. Sample was loaded on precast SDS PAGE gels and ran at 200V for 35min. Subsequently, the gel was stained with CoomassieBlue following the manufacturer and scanned to obtain gel image.

3.2 Cell biological methods

3.2.1 Eukaryotic Cell Culture

All cell lines used in this work are listed in **Section 2.12**. All cell lines were cultured in T25 or T75 cell culture flasks with corresponding cell culture mediums and cultured in 37°C incubator at 5% CO_2 atmosphere. All materials and media used during cell culture were previously either autoclaved for 20min at 121°C or sterile filtered. Work associated with cell culture were always carried out on a sterile workbench.

To passage cells, an aliquot of 1:5 to 1:10 diluted cell suspension was added into new cell culture flask every 2-3 days, and the ratio was depended on requirement and condition of cells. The adherent cell line HEK293-T was cultured in DMEM complete medium. These cells were first washed with $PBS^{-/-}$, then detached with 1ml (T25 flask) or 2.5ml (T75 flask) 1x trypsin at 37°C. Activity of trypsin was stopped by adding fresh medium, and cell suspensions were centrifuged to remove the trypsin containing supernatant. Cell pellets were resuspended in fresh medium and seeded in new cell

culture flasks. For the suspension cell line HEK293-6E, Freestyle 293 expression medium was used for cell culture and an aliquot of cell suspension was pass to new flasks in a ratio of 1:5.

Cell densities were determined with Neubauer counting chamber and the cell confluence was checked under microscope. The centrifugation parameters during cell culture were all 5min at 310rcf at 4°C. For T25 and T75 cell culture flasks, 5ml and 10ml cell culture medium were used, respectively.

3.2.2 Transient transfection of eukaryotic cells

The HEK293-T cells were prepared 1-2 days in advance, and transfection was performed when cell confluence was 70-80% and carried out with JetPEI (Polyplus) according to the protocol of manufacture.

The HEK293-6E cells prepared one day in advance, and the transfection was done with JetPEI according to the manufacturer. Cells were transfected for nanobody fragments production. The plasmids, cell lines and the particular purpose of transfection are listed in the following table.

Plasmid	Cell lines	Purpose
Human CD39-pCMV sport6	HEK293-T	Immunization/Selection/Functional assay
Mouse CD39-pCMV sport6	HEK293-T	Immunization/Selection/Functional assay
Human CD73-pCMV sport6	HEK293-T	Immunization/Selection/Functional assay
Mouse CD73-pCMV sport6	HEK293-T	Immunization/Selection/Functional assay
Nanobody-pCSE2.5_Rb Fc	HEK293-6E	Nanobody production

3.2.3 Stable transfection of eukaryotic cells

After transfection on HEK293-T cells as mentioned in **Section 3.2.2**, cells were kept in culture. 2-3 days after transfection, the cells were harvested and stained with corresponding antibodies. Only high expression cells were sorted by FACS Aria-IIIu Sorter. The sorted cells were kept in culture for around 1 week, and repeated sorting procedure 3-4 times until HEK293-T cells had a stable high expression of interested molecular.

3.3 Phage display associated methods

3.3.1 Preparation of nanobody immune repertories

After cDNA immunization using a GeneGun and transfected HEK293-T cell booster immunizations of three alpacas, blood was drawn from the alpacas SAL009, SAL010 and SAL0112 and RNA was prepared by EuroGentech.

By reverse transcription and PCR, the nanobody immune repertoires were amplified. For the amplification of nanobodies, primers IgG2b_rev/IgG2c_rev and SHF/LHF were used. Amplification products whose size were about 500bp were purified by gel purification. The amplicons and pHEN2 phagemid were digested with same restriction endonucleases and purified by gel purification. Subsequently, digested inserts and vector were ligated. Ligation products were used to transform TG1 cells, and transformed bacteria were plated on LB^{+Carb} agar plates. Eventually, the plates were scraped and further stored at -80°C as a bacterial library.

3.3.2 Phage Library Production

The bacterial library was inoculated and cultured in 5ml $2\times YT^{Carb+2\%Glucose}$ medium (37°C, 150rpm) until OD600 = 0.5. Subsequently, the preculture was centrifuged (4600rpm, 10min, 4°C) and resuspended in 10ml $2\times YT^{Carb+2\%Glucose}$, followed by an incubation (37°C, 200rpm) until OD600 = 0.5. 5ml cultures were superinfected with 160µl M13K07 helper phage and incubated (30min, 37°C, 150rpm). The cultures were centrifuged (4600rpm, 10min, 4°C) and resuspended in 50ml $2\times YT^{Carb/Kana}$ to select bacteria that were co-transfected with phagemid and helper phage. The phages were produced subsequently (6h, 28°C, 220rpm).

After incubation for phage production, bacteria were pelleted by centrifugation (4600rpm, 10min, 4°C). 40ml supernatant which contained the produced phages were added to 10ml chilled PEG/NaCl buffer to precipitate the phages and were incubated on ice overnight. Subsequently, precipitated phages were pelleted by centrifugation (4600rpm, 10min, 4°C) and supernatant was discarded. The phage pellet was then resuspended in 1ml PBS and transferred to a 1.5ml reaction tube where 250µl PEG/NaCl buffer was added. After centrifugation for 5min at 13,000rpm at 4°C, the supernatant was transferred to a new tube that contained 250µl PEG/NaCl buffer. The centrifugation and transfer steps were repeated until no pellet was visible after centrifugation. Eventually, the purified phages were stored as phage library at 4°C.

3.3.3 Panning

To select specific nanobodies by phage display, HEK293-T cells which express the

target proteins (human CD39, mouse CD39, human CD73 and mouse CD73) and untransfected HEK293-T cells were used. First, in order to minimize nonspecific binding of the phage to the polystyrene surface of the falcon tube, 200µl of the phage library were blocked in 1.8ml blocking buffer for 1h at RT. The blocking buffer-phage mixture was added to untransfected HEK293-T cell suspension and rotated for 1h at 4°C to remove phages that bound to HEK293-T cell associated cell surface proteins. The cell suspension was centrifuged (4600rpm, 10min, 4°C) and supernatant was used to resuspend corresponding target protein transfected HEK293-T cells, this step was performed on a vibration shaker for 1h at RT. The cell suspension was then centrifuged (4600rpm, 10min, 4°C) and the supernatant was discarded. The cell pellet was washed for 15-20 times with 10ml blocking buffer. The cell pellet was resuspended with 1ml PBS and spun down (2500rpm, 5min, 4°C), and the supernatant was discarded. Elution of the phage was carried out by resuspending pellet in 500µl 1x trypsin and incubate for 15min at RT. The phage suspension was then added to a new 1.5ml tube which was pre-coated with 50µl 100mM AEBSF to neutralize trypsin. Sample were spun down (13000rpm, 5min, 4°C) with the eluted phages being in the supernatant.

3.3.4 Reinfection and expansion of selected phages

2.5ml TG1 cells with an optical density of OD600 = 0.5 were transfected with 500µl eluted phages and incubated for 30min at 37°C, then plated on 2×YT agar$^{Carb+2\%Glucose}$ and incubated at 37°C overnight. Colonies on plates were counted, and some colonies were picked for plasmid purification. The rest of the colonies were scraped from plates in 10ml 2×YT medium$^{Carb+20\%Gly+2\%Glucose}$ and incubated at room temperature for 1h. Bacteria suspension was centrifuged (4600rpm, 10min, 4°C) and pellet was resuspended in 1ml 2×YT medium$^{Carb+20\%Gly+2\%Glucose}$. The putatively enriched bacterial library was stored at -80°C. The picked colonies were used for plasmid minipreparations, then the plasmid library (nanobody library) was sequenced to obtain nanobody sequence information. The bacterial library was further used for phage production (see **Section 3.3.2**). The new phage library was used for another round of bio-panning as described in **Sections 3.3.2 and 3.3.3** in order to obtain a further enrichment of specific clones.

3.4 Production of nanobody-Fc fusion proteins (Nb_Fc)

As mentioned in **Section 3.3.4**, the nanobody library was sequenced. Since the plasmid backbone was the phagemid pHEN2 vector, primer LMB3 was used for sequencing. To better understand the specificity and function of promising selected nanobody candidates, they were produced as nanobody Nb-Fc in HEK293-6E cells. For this purpose, the nanobody library (in pHEN2 vector) was amplified by PCR with primer TE155 and TE156 through which only VHH fragments would be amplified. The VHH fragments were purified by gel purification and were digested with restriction endonucleases PciI and NotI for 2h at 37°C. The pCSE2.5 vector, containing CH2 and CH3 domains of the antibody Fc part of rabbit IgG were located on the downstream of NotI restriction cite, was digested by NcoI and NotI restriction enzymes and purified. Subsequently, the digested VHH fragments were ligated with digested pCSE2.5 vector backbone (**Sections 3.1.5-3.1.6**). After ligation and transformation into XL1 blue E.coli, plasmid minipreparations were performed and the correct sequences were verified by Eurofins. Successfully recloned nanobodies were hereafter produced in HEK293-6E cells.

To produce Nb_rbFc, 10µg plasmid was used to transfect HEK293-6E cells in a T75 cell culture flask (**Section 3.2.2**). One day after transfection, 250µl feeding medium was added. On the sixth day after transfection, the supernatant of cell suspension was harvested after centrifuged (4600rpm, 10min, 4°C). Eventually, the supernatant was sterile filtered through a Steriflip and stored at 4°C.

3.5 Fluorescence-activated cell sorting

3.5.1 Cell staining

Cells were resuspended in FACS buffer and incubated with corresponding antibodies at 4°C for 30min. Cells were washed (1410rpm, 5min, 4°C) twice with FACS buffer and resuspended in FACS buffer for measurement. If nanobodies or unconjugated primary antibodies were used for staining, secondary antibodies were needed. Anti-rabbit IgG(H+L) secondary antibodies were used if samples were pre-stained with Nb_rbFc. However, when samples were pre-stained with unconjugated primary antibody, a specific secondary antibody which was anti IgG(H+L) of primary antibodies were used. The secondary antibody staining was performed at 4°C for 30min, and following washing and resuspension steps were same as described above.

3.5.2 FACS analysis

After cell staining as described in **Section 3.5.1**, samples were measured on BD FACS Celesta. FACS Diva Software was used to perform the analyses nanobody binding to HEK293-T cells, human peripheral blood mononuclear cell (PBMC) or mouse spleen cells. FACS Aria-IIIu sorter was used to isolate transfected HEK293-T cells for obtaining HEK cells stably expressing a specific target antigen. The results were analyzed by Flowjo.

3.6 Nanobody binding assays

3.6.1 Screening Nanobody binding on stably transfected HEK293-T cells

Stably transfected HEK293-T cells (mouse and human CD39 and CD73) were harvested and cell counts were adjusted to 100 cells/ml. In order to allow analyses of e.g. binding of nanobodies to mouse and human CD39 and CD73 simultaneously, same amount of mouse and human CD39 and CD73 transfected HEK cells were differentially stained with corresponding cell proliferation dye (mouse CD39 (eFlour450-eFlour670-), human CD39 (eFlour450+eFlour670-), mouse CD73 (eFlour450-eFlour670+) and human CD73 (eFlour450+eFlour670+)) for 10min on ice. Subsequently, cells were washed (1410rpm, 5min, 4°C) with 10ml FACS buffer three times, and four HEK cell lines were mixed and incubated with nanobodies as described in **Section 3.5.1**. Nanobody binding capacity was measured by FACS.

3.6.2 Screening Nanobody binding on primary human and mouse cells

Human PBMCs were extracted from human peripheral blood, and mouse cells were isolated from mouse spleen. Human PBMCs and mouse spleen cells were stained with corresponding nanobodies/antibodies for regulatory T cells and CD8 T cells population gating (see **Section 3.5.1**). Nanobody binding capacity was measured by FACS.

3.7 Nanobody functional assay

3.7.1 Functional assay for CD39 specific nanobodies

CD39 is an ATP degrading ecto-enzyme. In order to measure extracellular ATP level, CellTiter-Glo® Luminescent Cell Viability Assay Kit (CTG, Promega) was used. Here, extracellular ATP is used by a luciferase to emit luminescent signals, which directly correlates with the amount of ATP extracellular.

Human or mouse CD39 stably transfected HEK293-T cells were harvested and cells

were put onto a 96-well plate (150µl per well) at a certain cell number. 50µl ATP was added to a final concentration of 50µM per well and incubated at room temperature for 30min. Then the plate was spun down (1410rpm, 5min, 4°C) and 50µl supernatant was transferred to a 96-well white 96-well-plate. Subsequently, 50µl CTG reagent was added per well, after 10min stabilization, luminiscence signal was measured by luminometer.

When performing functional assay of CD39 specific nanobodies, CD39 transfected HEK293-T cells were resuspended in 140µl medium and incubated with 10µl nanobodies on ice for 30min before adding ATP.

3.7.2 Functional assay for CD73 specific nanobodies

CD73 can generate adenosine from AMP. Thus, CD73 function was tested by high performance liquid chromatography (HPLC) to identify the amount of substrate etheno-AMP (eAMP) and the metabolite etheno-adenosine (eAdo). Alternatively, AMP-Glo assay kit (Promega) was used to analyse the capacity of CD73 in AMP degradation.

HPLC: $1x10^5$ mouse CD73 transfected HEK293-T cells were used per condition and resuspended in 150µl PBS. eAMP was added per condition to a final concentration of 1µM and incubated at 37°C for 1h. Supernatant were then harvest via centrifugation (450g, 5min, 4°C) and frozen at -20°C. HPLC measurement was performed by AG Tolosa.

AMP-Glo assay: 5,000 human CD73 transfected HEK293-T cells were used per well and resuspended in 150µl complete cell culture medium. Subsequently 100µl AMP were added to a final concentration of 10µM and incubated at room temperature for 40min. Cells were spun down (1410rpm, 5min, 4°C) and 25µl supernatant was transferred to a solid white 96-well-plate. 25µl AMP-Glo Reagent I were added per well, mixed and incubated at room temperature for 30min. This was followed by addition of 50µl AMP-Glo™ Detection Solution per well and incubation for 60min at room temperature. Plate was read with a plate-reading luminometer.

4. Results

The results of this thesis are divided into three subsections. The first subsection describes the preparation of recombinant plasmids and generation of stably transfected HEK293-T cells. The second subsection describes, which resembles the main part of this thesis, highlights alpaca immunization and nanobody selection by phage display. In the third subsection, selected nanobodies against mouse/human CD39/CD73 were analyzed towards their potential to down modulate the enzymatic activity of their targets.

4.1 Generation and characterization of mouse and human CD39/CD73 expressing HEK cell lines

4.1.1 Construction of expression plasmids for mouse and human CD39/CD73

Expression plasmids for human CD39, mouse CD73 and human CD73 were generated in the context of this thesis. The expression plasmid for mouse CD39 (pCMV sport6 vector backbone) was kindly provided by the lab of Prof. Koch-Nolte. Amino acid sequences of mouse CD73, human CD73, and human CD39 were obtained from Pubmed->Protein (NCBI reference sequence: huCD39: NP_001157650.1; msCD73: NP_035981.1; huCD73: NP_002517.1). Specie optimized reverse translation was conducted to acquire corresponding cDNA sequences. As shown in **Figure 4.1A**, these sequences were artificially equipped with flanking EcoRI and NotI restriction sites, eukaryotic expression Kozak sequence, and start and stop codons. These in silico designed sequences were then ordered from *Invitrogen*. The DNA fragment sizes of huCD39, msCD73 and huCD73 are 1600bp, 1762bp and 1756bp respectively. The pCMV sport6 vector and the to be inserted gene fragments were digested by EcoRI and NotI restriction enzymes (**Figure 4.1B**) and ligated (**Figure 4.1C**). To ensure ligation was successful, the ligated plasmids were sent for sequencing by *Eurofins*, using primers M13 forward and M13 reverse. Finally, according to sequencing results human CD39, human CD73 and mouse CD73 genes were all successfully inserted into pCMV sport6 vector.

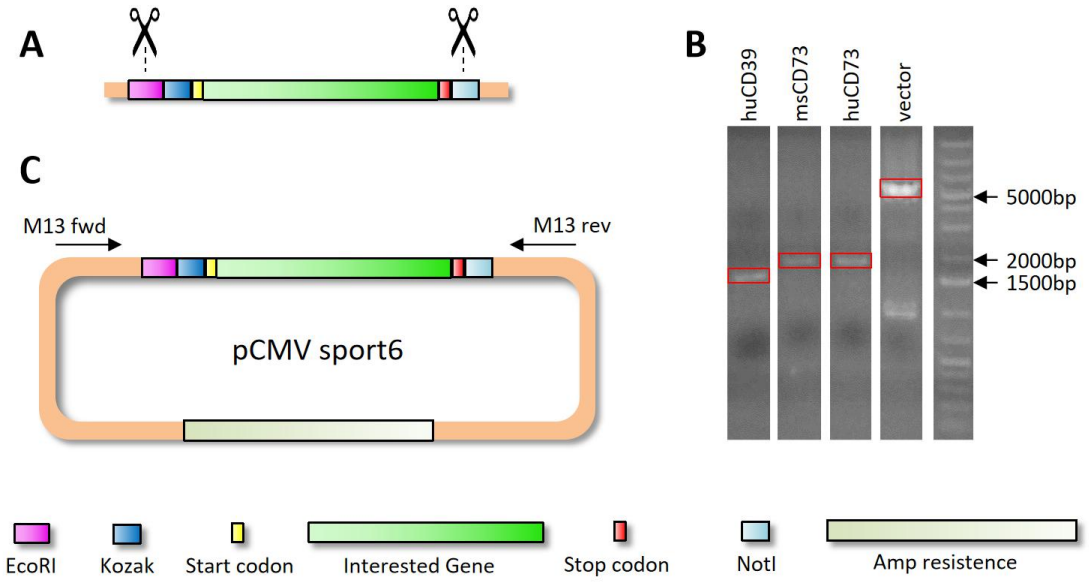

Figure 4.1: Cloning of human CD39, mouse CD73 and human CD73 genes into the pCMV sport6 vector. Engineered DNA sequence scheme (**A**). Constructs and pCMV sport6 vector were digested with EcoRI-HF and NotI-HF restriction enzymes and loaded on 1% agarose gel. The vector backbone and interested genes were collected from agarose gel (**B**). Digested constructs and vector backbone were purified via gel purification and ligated by T4 ligase. (**C**) shows the scheme of a successfully recombined plasmid.

4.1.2 Generation of ecto-enzyme expressing HEK293-T cell lines

HEK293-T cells were transfected with mouse CD39 and/or CD73 or human CD39 and/or CD73 encoding plasmid using JetPEI. Since CD39 and CD73 are both ecto-enzymes on cell membrane, surface staining with anti-CD39 and/or anti-CD73 antibodies was performed to analyze cell surface expression levels. Only HEK293-T cells with high fluorescence intensity were sorted for further culture, and this sorting process was done every 3-7 days until approximately 90% HEK293-T cells exhibited stable express of the desired protein. Eventually, huCD39, huCD73, msCD39, msCD73, huCD39/CD73, and msCD39/CD73 stably transfected HEK293-T cells were successfully generated (**Figure 4.2**).

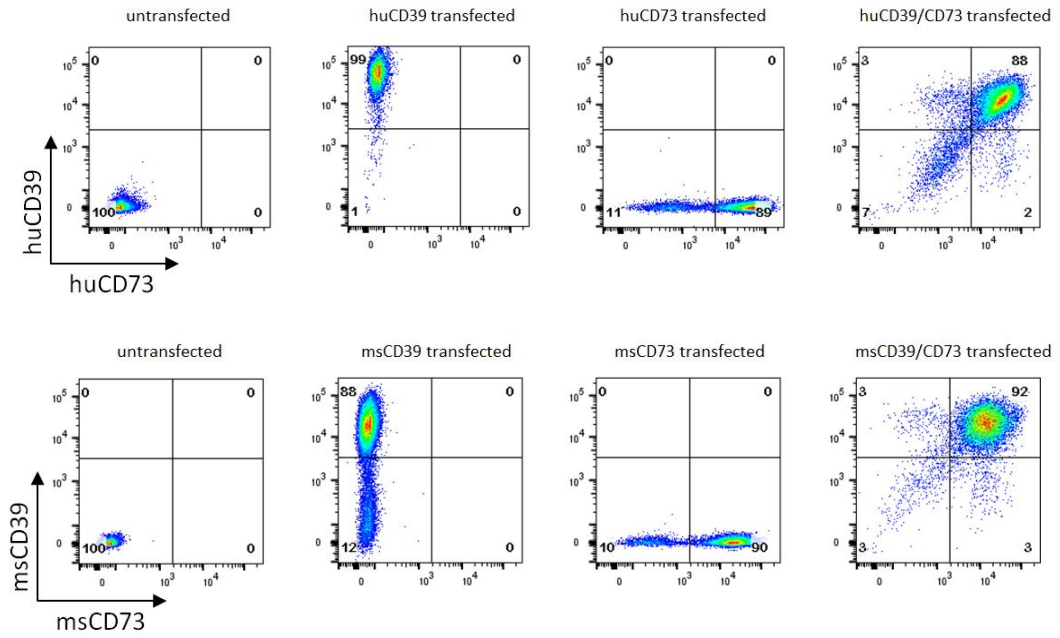

Figure 4.2: Generation of stably transfected HEK cell lines. Transient transfection with human or mouse CD39 and/or CD73 recombinant plasmid was performed. Cell surface staining with corresponding mAbs was done at 4°C for 30min, and samples were washed twice with FACS buffer. To obtain stably transfected HEK cell, cell population with high fluorescence intensity were sorted and kept in culture for next sorting. The process was repeated 3-5 times until approximately 90% cells highly expressed human CD39, human CD73, human CD39 and CD73, mouse CD39, mouse CD73 or mouse CD39 and CD73.

4.1.3 Characterization of ecto-enzyme expressing HEK293-T cell lines

To ensure CD39 and/or CD73 expressed on stably transfected HEK293-T cells retained their enzymatic function, functional assays monitoring the degradation of ATP as readout for CD39 function and the generation of adenosine as readout for CD73 function were performed. For human and mouse CD39 transfected HEK293-T cells, CellsTiter-Glo Kit (CTG, Promega) was used, where a luciferase generates a luminescent signal being proportional to the available amount of extracellular ATP. Compared to untransfected cells, ATP decreased significantly after incubating with either human CD39 or mouse CD39 transfected HEK293-T cells. This was also depending on the number of cells used for this assay: a minimum of 1000 CD39-transfected HEK cells still substantially reduced the amount of extracellular ATP, whereas 10,000 cells almost completely degraded the available extracellular ATP (**Figure 4.3A**).

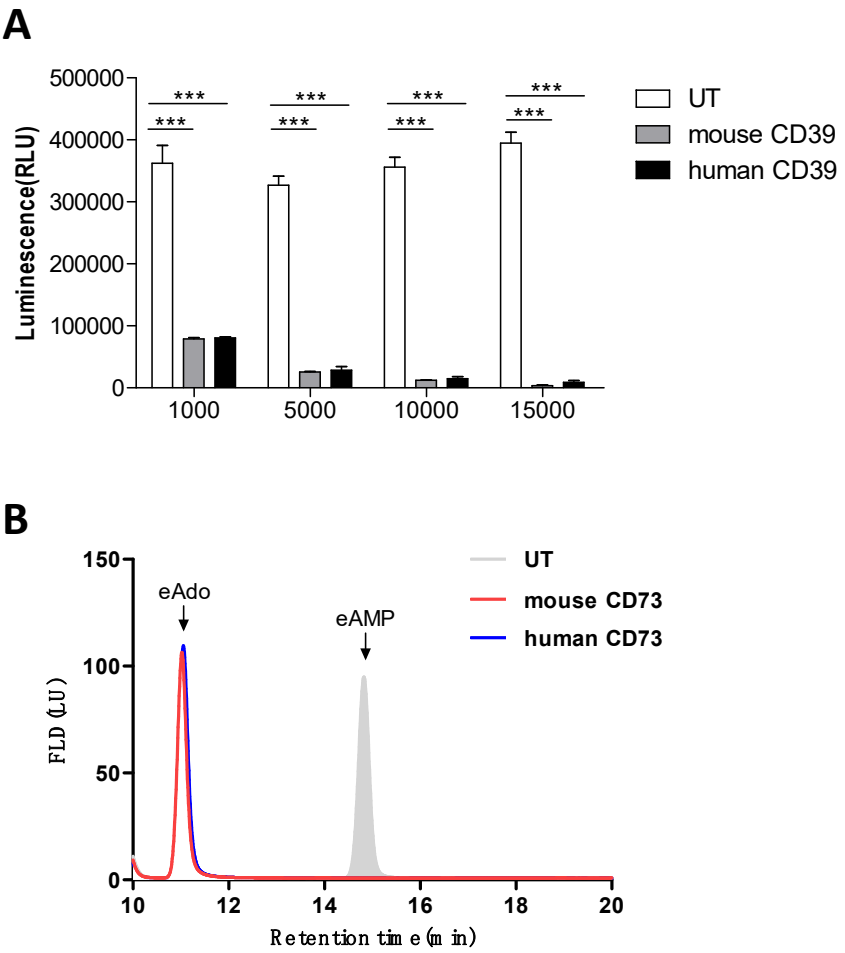

Figure 4.3: Monitoring the enzymatic activity of CD39/CD73 stably transfected HEK293-T cells. **(A)** Different cell amounts, 1000, 5000, 10000 and 15000 cells were used respectively. ATP with a final concentration of 50µM was added to cells and incubated at 37°C for 30min. Samples were spun down and 50µl supernatants were transferred to a 96-well white plate. After addition of 50µl CTG reagent, luminescent signal was measured on luminometer. **(B)** $1x10^5$ huCD73, msCD73 and untransfected HEK293-T cells were resuspended with 150µl PBS respectively, 50µl eAMP (final concentration 1µM) was added and incubated at 37°C for 30min, subsequently samples were spun down and 200µl supernatants were harvested for HPLC measurement.

For analyzing CD73 enzymatic activity, an HPLC assays was performed to monitor the conversion of etheno-AMP (eAMP) to etheno-adenosine (eAdo). Of note, in untransfected HEK293-T cells, eAMP was not degraded and no adenosine was generated. In contrast, eAMP was completely converted to eAdo by both, human and mouse CD73 transfected HEK293-T cells (**Figure 4.3B**).

4.2 Selection of CD39 and CD73 specific nanobodies from immunized alpacas

4.2.1 Alpaca immunization and phage library generation

To induce the generation of anti-CD39 and anti-CD73 immunoglobulins in alpacas *in vivo*, the animals named SAL009, SAL010 and SAL012 were immunized by gene gun with mouse and human CD39 and CD73 encoded plasmids conjugated to gold particles, followed by three gene gun booster immunizations on days 21, 42 and 64, and a final protein boost with CD39/CD73 transfected HEK cells on day 85 (**Figure 4.4A)**. Peripheral blood was drawn on days 70 and 91 (Blood1 and Blood2). B cells were isolated from Blood1 and Blood2, mRNA was extracted from B cells and reversely translated to cDNA fragments. The nanobody repertoire was amplified from IgG2b and IgG2c, which form alpaca heavy chain antibodies, by PCR using IgG2b_rev/IgG2c_rev and SHF/LHF primers. During the PCR amplification process, SfiI and NotI restriction sites were introduced to terminals of nanobody sequences. The nanobody repertoires and phagemid pHEN2 were cut by SfiI and NotI restriction enzymes and ligated by T4 ligase (**Figure 4.4B**). TG1 were transduced with recombinant phagemid, and phage libraries were successfully produced with the help of helper-phages. Nanobodies were expressed as phage coat protein III fusion proteins.

Next, phage display was performed on CD39 or CD73 stably transfected HEK293-T cells, and corresponding nanobody-expressing phage libraries were panned to acquire specific nanobodies (**Section 3.3**). The 1st round of panning was performed on mouse or human CD39/CD73 stably transfected HEK293-T cell lines respectively. Strikingly, after one round of panning, selection on mouse CD39, human CD39 and mouse CD73 resulted in the enrichment of nanobody families containing potential binders against their specific target. For huCD73, the majority of selected nanobodies from SAL009 belonged to the same family. In order to obtain more specific families, a 2nd round of panning was performed on huCD73 HEK293-T cells, with cells being preincubated with dominant family of panning round one, in order to block that specific epitope.

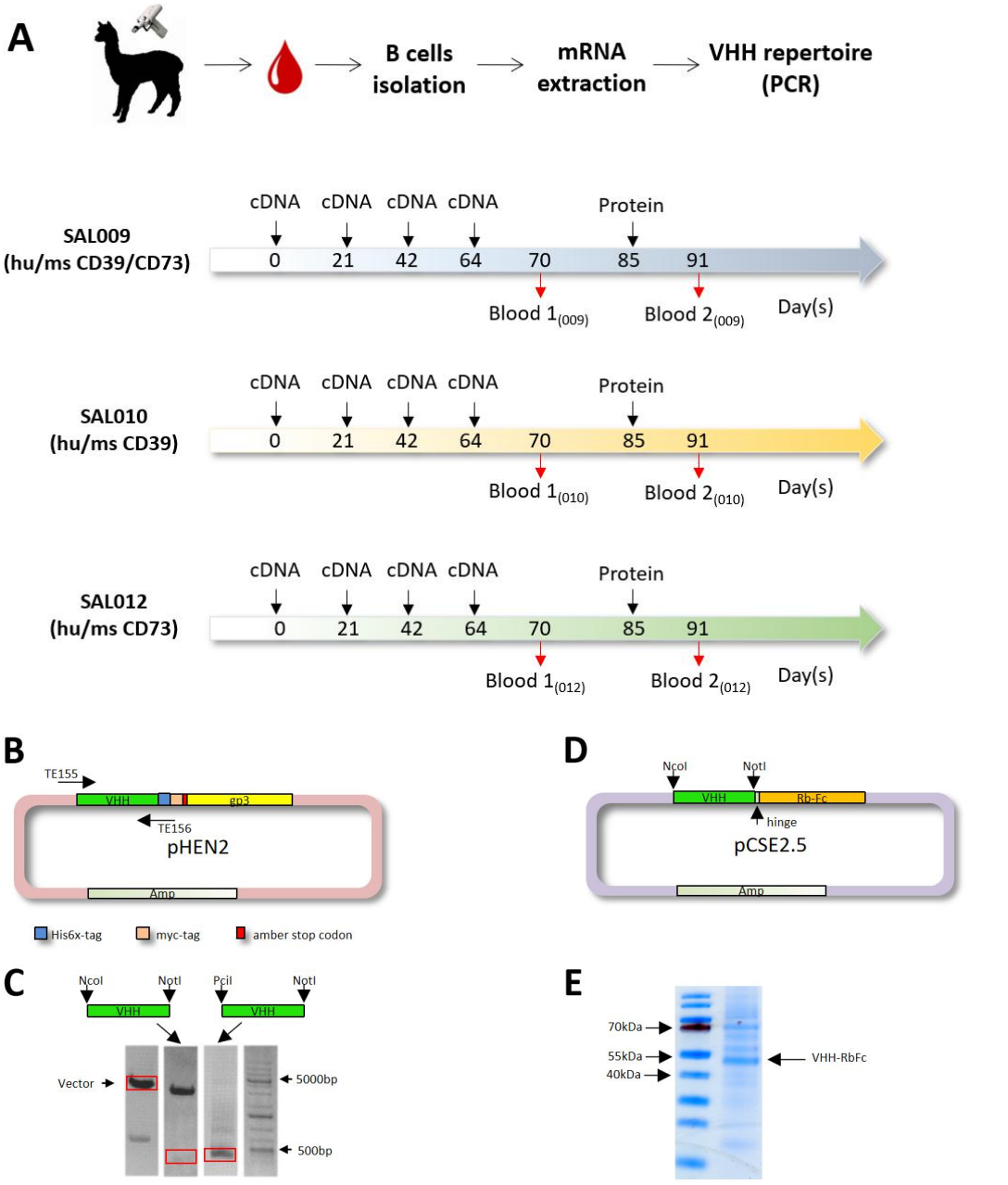

Figure 4.4: Immunization schematic and Nb_rbFc production. (**A**) Alpaca immunization scheme. SAL010 was immunized with mouse and human CD39, SAL012 was with mouse and human CD73, while SAL009 was immunized with all four target proteins. The immunization schedule for three alpacas were the same: first, alpacas were 4x immunized with recombinant plasmids via gene gun, and peripheral blood was drawn 7 days after the last cDNA immunization (Blood 1). Then stably transfected HEK293-T cell immunization were performed and blood was drawn 7 days later (Blood 2). (**B**) Nanobody repertoire was inserted into pHEN2 phagemid vector. His6x, myc tags and amber stop codon were arranged between nanobody and gp3 sequences. Primers TE155 and TE156 were used to amplify the nanobody sequence that had internal NcoI restriction site, which replaced the restriction site NocI at the begnning of VHH fragment by PciI. (**C**) pCSE2.5_rbFc vector and nanobody sequence which were without NocI internal restriction site were digested by NcoI-HF/NotI-HF restriction enzymes. PciI and NotI restriction enzymes were used for digestion if there was internal NocI restriction site in nanobody sequence . The size of vector backbone and nanobody were approximately 5000bp and 500bp respectively. The DNA bands at the correct size were extracted and purified for ligation. (**D**) Scheme of ligated nanobody and vector backbone. (**E**) Nb_rbFc were denatured before loading on SDS-PAGE, and the present band at about 55kDa indicates a successful production of Nb_rbFc.

In order to investigate the specificity of selected nanobodies, one or more clones from each family were cloned into a plasmid optimized for recombinant protein expression in eukaryotic cells. First, nanobodies were recloned into eukaryotic expression vector pCSE2.5_rbFc. When nanobody sequences had no internal NocI restriction site, digestion was conducted directly with NcoI and NotI restriction enzymes. However, when nanobody sequence had an internal NcoI restriction site, nanobody sequences were first amplified by primers introducing PciI and NotI flanking the nanobody sequence (**Figure 4.4B**). Since NcoI and PciI enzymes are isocaudomers which generate the same sticky ends, NcoI (and PciI)/NotI digested nanobody sequences were ligated to NcoI/NotI digested pCES2.5_rbFc vector (**Figure 4.4C and D**). To produce Nb_rbFc, HEK-6E cells were transfected with recloned plasmids. Cell culture medium supernatant was harvested and loaded on SDS-PAGE to ensure whether the fusion antibodies were successfully produced (**Figure 4.4E**).

4.2.2 CD39/CD73 specific nanobodies bind to CD39/CD73 transfected HEK293-T cells

In order to investigate the specificity of the selected nanobodies, screening on stably transfected HEK293-T cells was performed. Since we would like to obtain the specificity of each nanobody to different cell lines, cell proliferation dyes provide the possibility to achieve this simultaneously. Cells labelled with cell proliferation dye can be tracked for a long term and detected by FACS. Therefore, if cells are pre-stained with different comparable cell proliferation dyes, after mixing cell populations can be distinguished by FACS. In this study, four stably transfected HEK293-T cell lines (mouse CD39, human CD39, mouse CD73 and human CD73) were labelled with cell proliferation dye eFluo670 and/or eFluor450 accordingly and mixed (**Section 3.6.1**). This cell mixture was first incubated with recombinant Nb_rbFc candidate. After washing away unbound Nb_rbFc, cells were stained with anti-rabbit IgG(H+L) secondary antibody. Subsequently, the binding specificity and intensity of antibody were measured via flow cytometry (**Figure 4.5**).

This screening resulted in the identification of 11 and 9 families of specific binders to CD39 and CD73, respectively. Four families were specific for mouse CD39, six families were specific to human CD39 and one family was cross-reactive to mouse and human CD39. The majority of the CD39 specific families showed a strong signal on the transfected HEK293-T cells, only fam1 and fam2 gave a moderate binding

signal. The cross-reactive family fam3 showed a strong signal on msCD39 HEK293-T cells and a weak signal on huCD39 HEK293-T cells (**Figure 4.5, Table 4.1**). For CD73, three mouse CD73 and three human CD73 specific families and three cross-reactive families were identified upon phage display screening. The majority of these clones showed prominent signals on transfected HEK293-T cells, only two clones from fam18.3 (18-1 and 18-8) gave intermediate signals on mouse CD73 HEK293-T cells. In addition, several clones from fam22 (22-1, 22-1, 22-3 and 22-5) gave only a weak signal on mouse and human CD73 HEK293-T cells (**Figure 4.5, Table 4.2**).

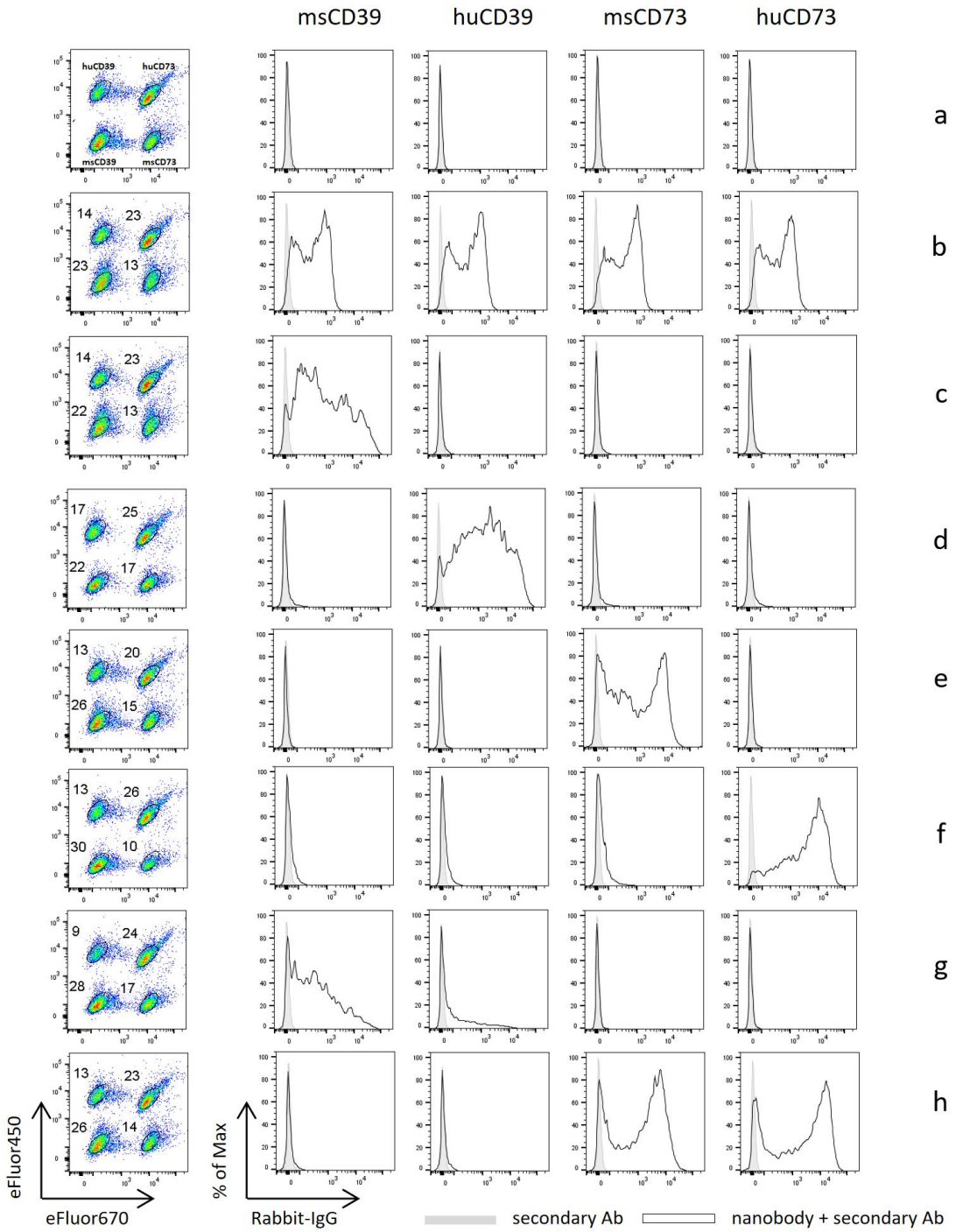

Figure 4.5: Binding of Nb_rbFc fusionproteins to mouse/human CD39/CD73 stably transfected HEK293-T cells. Mouse and human CD39/CD73 single transfected HEK293-T cell lines were differentially labeled with eFluor450 and/or eFluor670 as shown in left and mixed in equal ratios (200,000 cells). Mixed cells were incubated with Nb_rbFc generated after phage display, and bound Nb_rbFc were detected via fluorochrome conjugated anti-rabbit IgG(H+L) secondary antibody. **(a)** A non-binding nanobody which binds to none of the transfected cell lines; **(b)** A sticky nanobody that can bind to all transfected cell lines; **(c)** A mouse CD39 specific binder; **(d)** A human CD39 specific binder; **(e)** A mouse CD73 specific binder; **(f)** A human CD73 specific binder; **(g)** A mouse and human CD39 cross-reactive binder; **(h)** A mouse and human CD73 cross-reactive binder.

Table 4.1 CD39 specific nanobody families

Antigen	Fam.	ERSI name	# mutation vs parent	CDR3 domain	Intensity	Alpaca
msCD39	2	2-1		DLYTYCSDSSSTR	++	SAL009
	10	10-1		IGANY	++++	SAL009
	13	13-2	1	KVDGLGLTSNEYQH	++++	SAL010
		13-5	10	KVDGLGYTSNEYHY	++++	SAL009
		13-7	9	KVDGLGYTSREYQY	++++	SAL009
		13-9	7	KVDGLGTTSNEYQY	+++	SAL009
		13-10	4	KVDGLGYTSNEYQH	+++	SAL009
		13-11	7	KVDGLGYTSNEYQY	+++	SAL009
		13-12	1	KVDGLGTTSNEYQH	+++	SAL009
		13-13	3	KIDGLGTTSNDYQH	++++	SAL009
		13-15	9	KVDGLGYTSTEYQY	++	SAL009
		13-16	7	KVDGLGYTSKEYQV	+++	SAL009
		13-17	11	KLDGLGYTSNEYHY	+++	SAL009
	16	16-1		NFLGIEY	+++	SAL009
		16-2	6	NFLGMEY	++++	SAL009
		16-3	3	NFLGMEY	++	SAL009
huCD39	1	1-1		AYGGRSVVAQTA	++	SAL010
	7	7-1		GDSGA	+++	SAL009
	11	11-4	10	IGGSTWFGEDEPDY	+++	SAL009
		11-5	9	IGGSTWFGEDEPDY	++++	SAL010
		11-6	12	IGGSTWFGEDEYDN	++++	SAL010
		11-7	7	IGGSTWFGEDEYDY	+++	SAL010
		11-8	10	IGGSTWFGEEEYDS	++++	SAL010
	15	15-1		KYSRYAPQSTDYDY	++++	SAL009
		15-2	3	KYSRYAPQSTDYDY	++++	SAL009
		15-3		KYSRYAPQSTDYDY	++++	SAL010
		15-5	8	KYSRYLPQSTDYDY	++++	SAL010
		15-8	10	KYSRYNLQSTDYDY	++++	SAL010
	17	17-1		NSRNTNYYRPNGYDY	+++	SAL009
	19	19-1		RAPRYGTASTRLSDYDN	+++	SAL010
ms/huCD39	3	3-1		DPNYGSSITSGYTY	(m/h) +++/+	SAL009

Table 4.2 CD73 specific nanobody families

Antigen	Fam.	ERSI name	# mutation vs parent	CDR3	Intensity	Alpaca
msCD73	8	8-1		GPPTSTPEE	++++	SAL009
		8-2	1	GPPTSTPEE		SAL009
	20	20-1		YYY	++++	SAL009
	18.1	18-6		QRRWNAY	++++	SAL009
huCD73	9	9-2	1	HKYYYCSNKVAVFDY	++++	SAL009
		9-3	5	HKYYYCSNKVEVFDY	++++	SAL009
		9-5	7	HKYYYCPNKVEVFDY	++++	SAL009
	18.2	18-2	9	QKYYYCSGKVEVYDY	++++	SAL009
		18-4	12	QKYYYCSRKGEVYDS	++++	SAL009
	21	21-1		SRDLFNEGEYDY	++++	SAL012
		21-2	1	SRDLFGEGEYDY	++++	SAL012
ms/huCD73	12	12-1		IPGND	(m/h) +++/++++	SAL009
	18.3	18-1		QKYYYCSGKAEVYDY	(m/h) ++/++++	SAL009
		18-3	10	QKYYYCSGRVEVYDY	(m/h) ++++/++++	SAL009
		18-7	10	QRYYYCSDKVAVYDY	(m/h) ++++/++++	SAL009
		18-8	7	QRYYYCSDKVEVYDY	(m/h) ++/++++	SAL009
	22	22-1		TAGGPYYLGGRDILYDY	(m/h) ++/++	SAL012
		22-2	7	TAGGPDYLGGRDIVYDY	(m/h) +/+	SAL012
		22-3	9	TAGGPDYLGGRDIVYDY	(m/h) +/++	SAL012
		22-4	1	TAGGPYYLGGRDILYDY	(m/h) +++/+++	SAL012
		22-5	3	TAGGPDYLGGRDTLYDY	(m/h) ++/+++	SAL012

4.2.3 CD39/CD73 specific nanobodies bind to primary human and mouse immune cells

The binding capacity of nanobodies was verified on primary human and mouse immune cells. Human peripheral blood mononuclear cells (PBMC) were isolated from donors, and $CD4^+CD25^+CD127^{low}$ Tregs and $CD8^+$ T cells were stained with corresponding mAbs. Human CD39 and human CD73 specific candidates were tested on Tregs and $CD8^+$ T cells separately. Mouse spleens were obtained from C57BL/6 mice and lymphocytes were extracted. $CD4^+CD25^+$ Tregs were used for analyzing the specificity of mouse CD39 and mouse CD73 nanobody candidates.

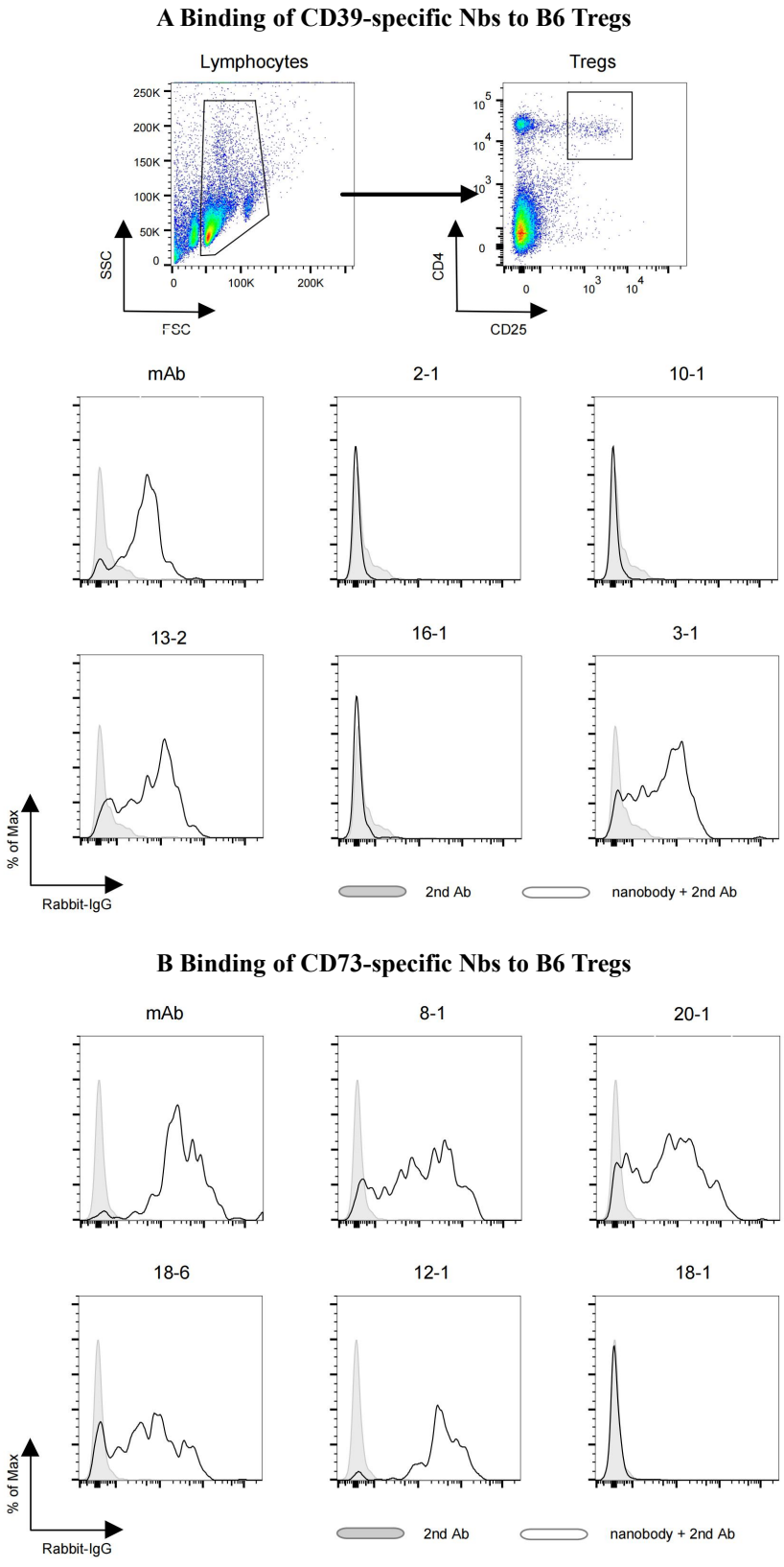

Figure 4.6 Screening of selected mouse specific nanobodies on primary mouse T cells. Mouse spleen lymphocytes were extracted and incubated with anti-CD4 and anti-CD25 mAbs to label regulatory T cells. This was followed with incubation of anti-CD39 or anti-CD73 mAbs, or corresponding CD39 specific nanobodies **(A)** or CD73 specific nanobodies **(B).** Afterwards the nanobody stained cells were incubated with anti-rabbit IgG secondary antibody and samples were measured by FACS.

4.2.3.1 Selected mouse CD39/CD73 specific nanobodies

All nanobodies that were positively evaluated to bind to msCD39 and msCD73 stably transfected HEK293-T cells were screened on primary mouse cells. Among selected msCD39 specific nanobodies, only fam13 and the cross-reactive fam3 could strongly bind to primary mouse Tregs, while other families (fam2, fam10 and fam16) didn't show any binding capacity (**Figure 4.6A**). For selected msCD73 specific nanobodies, majority of families (fam8, fam12, fam20 and fam18.1) could moderately bind to murine Tregs, only fam18.3 was unable to bind CD73 on primary cells (**Figure 4.6B**).

4.2.3.2 Selected human CD39/CD73 specific nanobodies

For evaluating the binding of selected human specific nanobodies to human immune cells, Tregs were used to analyze as source of CD39 expressing cells, whereas CD8 T cells were used as source of CD73 expressing cells. The results from the flow cytometric analyses show that all six mono-reactive anti-huCD39 families (fam1, fam7, fam11, fam15, fam17 and fam19) could bind to some extend to human CD39 on Tregs. Here, fam11 and fam15 exhibited robust labeling capacity of CD39-expressing Tregs. In contrast, fam1, fam7 and fam17 showed only moderate labeling capacity and incubation with fam19 resulted only in a very faint labeling of Tregs. Strikingly, the members of fam3 which exhibited cross-reactive binding capacity to mouse and human CD39 on transfected HEK cells were unable to bind to primary human Tregs (**Figure 4.7A**). For anti-huCD73 nanobodies, all identified human-reactive and human/mouse cross-reactive families exhibited a strong labeling capacity of CD73-expressing human CD8 T cells (**Figure 4.7B**).

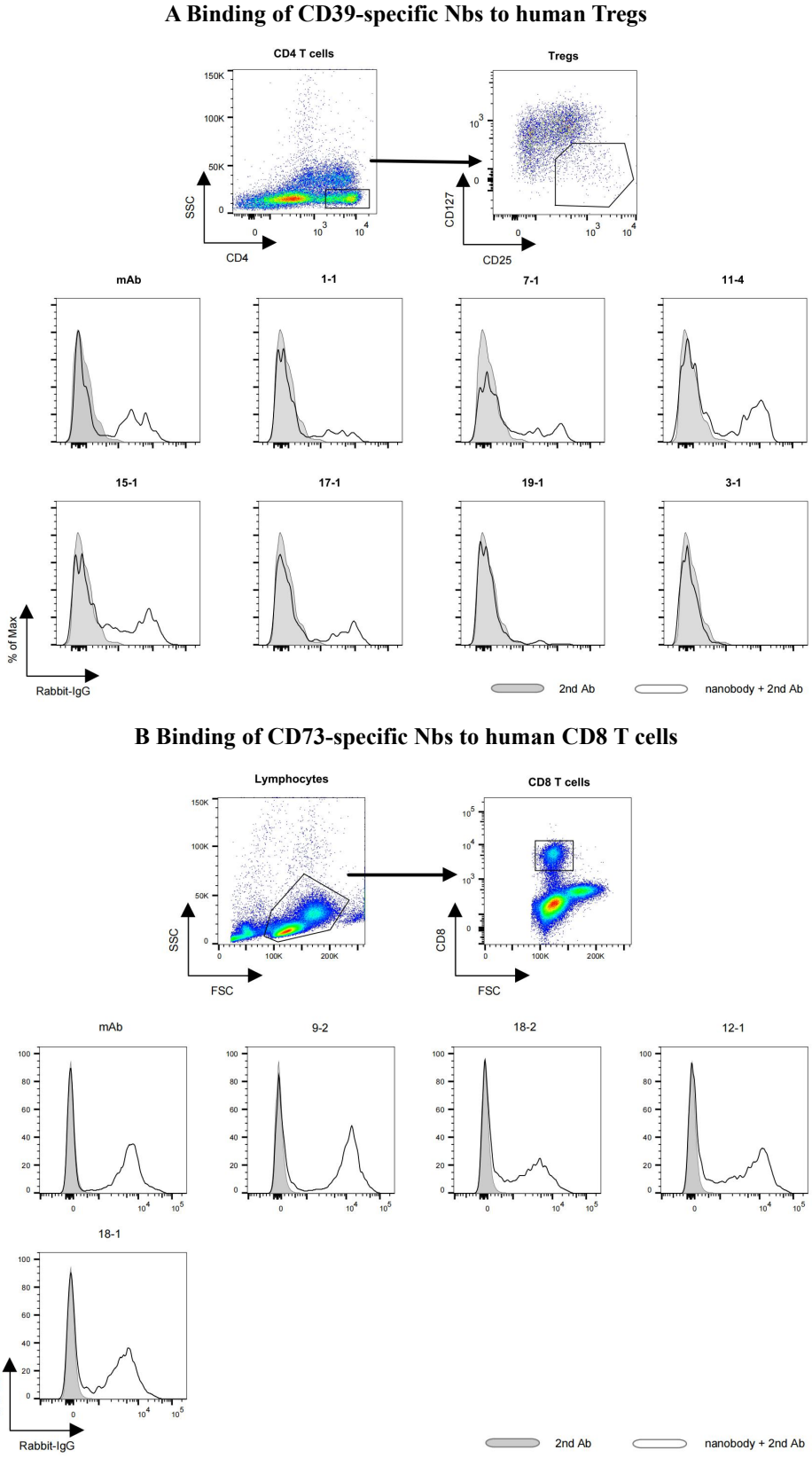

Figure 4.7 Screening of human CD39 or CD73 specific nanobodies on primary human cells. Human PBMC were isolated by Enja Schneider from the group of Prof. Eva Tolosa. Tregs and CD8 T cells were labeled by anti-CD4/CD25/CD127 and anti-CD8 mAbs respectively. This was followed by the incubation of anti-CD39 or anti-CD73 mAbs, or huCD39 specific nanobodies **(A)** or huCD73 specific nanobodies **(B).** Afterwards, the nanobody stained cells were incubated with anti-rabbit IgG secondary antibody, and samples were measured via FACS.

4.3 Functional characterization of anti-CD39 and anti-CD73 nanobodies

4.3.1 Identification of CD39-specific nanobodies that inhibit ATP degradation

Mouse and human CD39 specific nanobody functional assays were carried out on stably transfected HEK293-T cells and CTG assay kit (Promega) was used. In order to analyze the impact of the nanobodies on inhibiting or potentiating CD39 activity, mouse and human CD39 HEK293-T cells were pre-incubated with different nanobody clones before adding ATP. The luminescence signals obtained from untransfected (UT) HEK293-T and from CD39 transfected cells incubated with a non-binding control Nb were used as controls for no ATP degradation and maximum ATP degradation, respectively (**Figure 4.8A and B**). Among nanobodies specific for human CD39, fam11 and fam15 showed CD39 inhibitory properties, as they diminished the degradation of ATP. Fam17 and fam19 could slightly inhibit the degradation of ATP, but the rest of the tested nanobodies did not seem to affect ATP degradation (**Figure 4.8A**). For mouse CD39-specific nanobodies, fam2 exhibited potent CD39 inhibitory potential, while fam10 and fam16 moderately inhibited ATP degradation. Finally, the cross-reactive fam3 showed slight inhibition of mouse CD39 while it had no substantial impact on human CD39 activity (**Figure 4.8B**).

4.3.2 Identification of CD73-specific nanobodies that inhibit AMP degradation

A selection of CD73-specific nanobodies was evaluated towards their capacity to block the CD73-mediated conversion of AMP into adenosine. Four msCD73-specific nanobodies and five huCD73-specific nanobodies were included in this analysis. For mouse CD73 specific nanobodies, in line with CD73 HEK cells functional assay (**Section 4.1.3**), HPLC was used for the measurement. With this technique, AMP degradation and adenosine generation can be detected simultaneously by using fluorescent etheno-analgues (Menegollo et al. 2019). As shown in **Figure 4.9A**, mouse CD73 HEK cells ("control") converted all eAMP to eAdo, while PSB-14685, a potent CD73 inhibitor (Bhattarai et al. 2019) could completely inhibit mouse CD73 activity. Clone 18-6 could strongly exhibit CD73 activity but was slightly weaker than PSB-14685; clone 20-1 had moderate inhibitory effect (**Figure 4.9A**).

An alternative to the HPLC-based assay was invented by Mondal and colleagues, which is the AMPGlo assay that quantifies the amount of extracellular AMP (Mondal et al. 2017). This detection system converts AMP into ATP, which in turn is needed by

the luciferase in order to emit light in the presence of its substrate luciferin. Therefore, the luminescent signal is proportional to the amount of AMP and can be used to monitor the activity of CD73 towards AMP degradation. As shown in **Figure 4.9B**, AMP was almost entirely degraded by human CD73 HEK cells ("control") when compared to untransfected HEK cells (**Figure 4.9B**). All five human CD73 binders showed slightly inhibitory effect on CD73 activity in this AMP degradation assay.

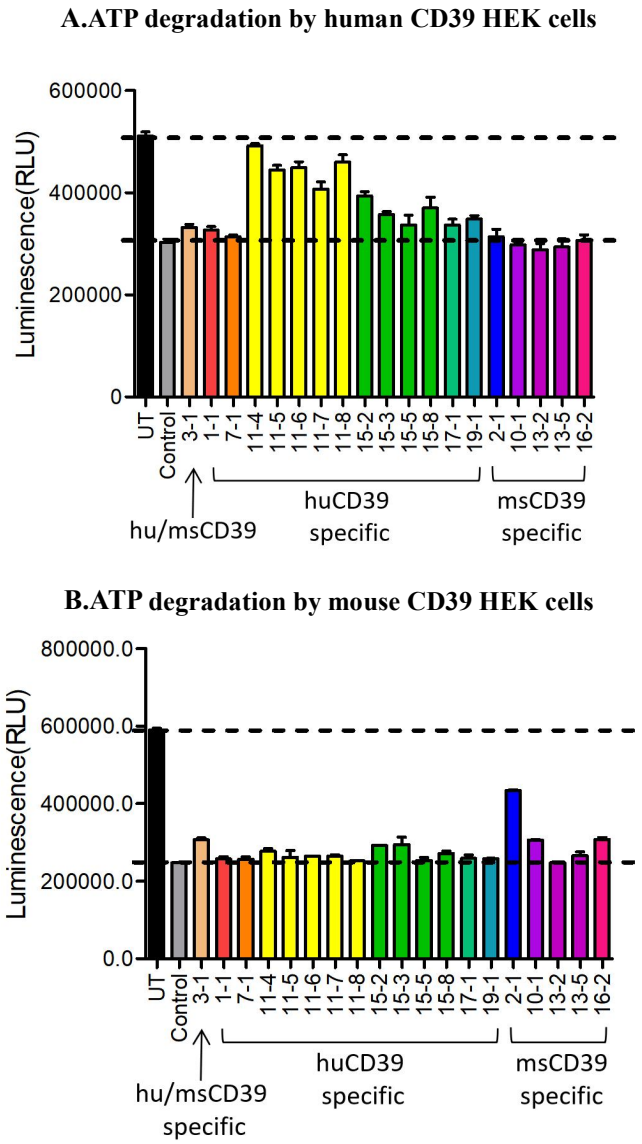

Figure 4.8 Probing CD39 specific nanobody for their potential to block CD39 activity. CD39 specific nanobody functional assays were performed on human CD39 (**A**) and mouse CD39 (**B**) stably transfected HEK293-T cells. Stably CD39 transfected HEK cells were harvested and 140µl cell suspension with 5000 cells were plated per well. 10µl supernatant of the production of the corresponding nanobody or control solution were added and incubated on ice for 30min. ATP was added to a final concentration of 50µM and cells were incubated at room temperature for 30min. Cells were spin down and 50µl supernatant was transferred to a solid 96-well plate. After the addition of 50µl CTG reagent and 10min of stabilization, the plate was read with a luminometer.

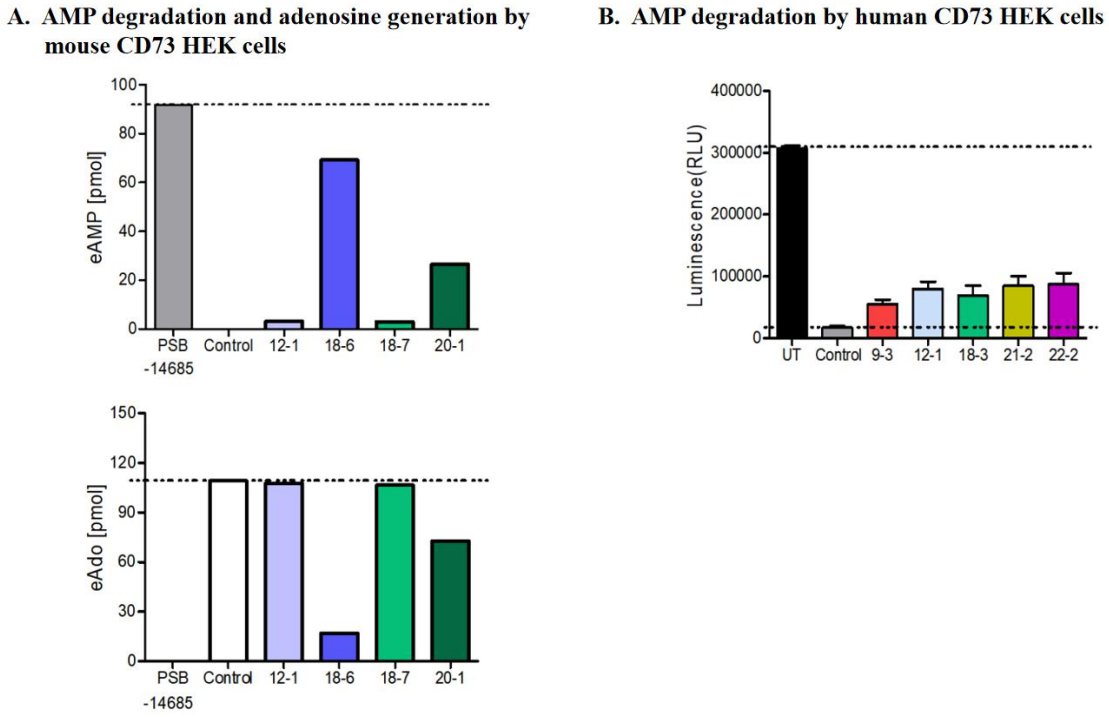

Figure 4.9 Probing CD73 specific nanobody for their potential to block CD73 activity (**A**) HPLC was used for functional assay of mouse CD73 specific nanobodies. $1x10^5$ msCD73 HEK293-T cells were resuspended in 140µl medium per condition. 10µl corresponding nanobody and PSB-14685 were added and incubated on ice for 30min. Addition of 50µl eAMP (final concentration 1µM) was followed and incubated at room temperature for 1h. PSB-14685 was added to stop the reaction. msCD73 HEK293-T cells were pelleted via centrifugation and supernatant was harvested for HPLC measurement. (**B**) 5,000 human CD73 transfected HEK293-T cells were used per well and resuspended in 140µl complete cell culture medium. 10µl corresponding nanobody were added and incubated on ice for 30min. 100µl AMP were added to a final concentration of 10µM and incubated at room temperature for 40min. Cells were then spun down (1410rpm, 5min, 4℃) and 25µl supernatant was transferred to a solid 96-plate for AMP-Glo assay.

5. Discussion

The goal of this study was to select nanobodies against mouse and human CD39 and CD73 from a phage VHH library generated from immunized alpacas. Promising binders were further screened towards their capacity to inhibit the enzymatic activity of CD39 or CD73, respectively. This resulted in the identification of numerous clones, specific for all four targets, some of which showed cross-reactivity between mouse and human CD39/CD73 orthologues. Finally, it could be demonstrated that some clones exhibited enzyme inhibiting capacity.

5.1 Generation of transfected HEK cells and their use for isolating antigen-specific nanobodies

CD39 and CD73 both are ecto-nucleotide enzymes, their enzymatic active sites locate and hide in the extracellular domains (refer to their 3D structures in UniProt). Since the paratope of conventional antibody is flat or concave, while the extended CDR3 facilitates nanobody forming a convex paratope (Jovčevska and Muyldermans 2020), the generation of nanobodies against CD39 or CD73 catalytic site seems to be a promising approach to block enzymatic activity. To date, various nanobodies that modulate enzymatic activity have been identified (Könning et al. 2017) (Zavrtanik et al. 2018).

For nanobody generation, dromedaries, bactrian camels, llamas or alpacas are most commonly immunized (Muyldermans 2021). Alpacas were used in this study. The amino acid sequences of mouse and human CD39 and CD73 differ from the alpaca orthologs (**Appendix 7.1 and 7.2**). When compared to alpaca, mouse and human CD39 amino acid sequences show 64.57% and 69.74% similarity, respectively, while the sequence similarity of mouse and human CD73 compared to alpaca CD73 is 85.02% and 91.29%, respectively. Since sequence and structural similarity between alpaca and the host of the desired target protein have a great impact on the immunogenicity of target protein, we were quite optimistic to isolate some clones against CD39 and CD73. In this study, mouse and human CD39 and CD73 expression plasmids as well as stably transfected HEK cells were used for alpaca immunization. With this immunization strategy, native conformations of CD39 or CD73 can be exposed to alpaca immune system (Eden et al. 2018), and this is important for i) getting nanobodies that bind to the native conformation of both enzymes and ii)

getting nanobodies with antagonist potential. In addition, this strategy also facilitates the elimination of nonspecific Nbs by pre-adsorption of Nb library against unstransfected HEK cells during panning.

In order to obtain enriched specific nanobodies, 2-3 rounds panning are generally needed (Muyldermans 2013). In this study, after one to two rounds of panning, 11 CD39 specific families and 9 CD73 specific families are identified, pointing towards a decent immune response of the immunized alpacas against these targets. The efficiency of this study towards the generation of target-specific nanobody families seems comparable to studies performing 3-4 rounds of enrichment (Li et al. 2012)(Schoonaert et al. 2017). Besides, the fraction of enzymatic inhibitors in all specific nanobody families is higher than studies which used recombinant enzymes for immunization (Gulati et al. 2018) (Simmons et al. 2021). The extended CDR3 of nanobodies selected in this study potentially contributes to their inhibitory capacities (Schumacher et al. 2018). As shown in **Table 5.1**, the length of CDR3 of identified nanobodies vary between 3 to 17 residues and the most potent inhibitors of each target (msCD39(fam2), huCD39 (fam11), msCD73 (fam18.1) and huCD73 (families expect fam18.2)) exhibit a relatively longer CDR3 which mainly ranges from 12-17 residues. This indicates that immunization with transfected cells is a powerful strategy to generate membrane protein specific nanobodies, especially when aiming to enzymatic inhibitors.

Table 5.1 Summary of CDR3 length of each family

Antigen	Fam.	Length of CDR3
msCD39	2	13
	10	5
	13	14
	16	7
huCD39	1	12
	7	5
	11	14
	15	14
	17	15
	19	17
ms/huCD39	3	14

Antigen	Fam.	Length of CDR3
msCD73	8	9
	20	3
	18.1	7
huCD73	9	15
	18.2	15
	21	12
ms/huCD73	12	5
	18.3	15
	22	17

5.2 The discrepancy of anti-mouse CD39 binding to transfected HEK cells and primary T cells

In this study, majority of mouse CD39 specific clones show high binding capacity to mouse CD39 transfected HEK293-T cells, however, these clones were unable to bind to primary mouse Tregs, which express high level of CD39. Therefore, either CD39 on the transfected HEK cells differs from the Treg CD39 in its posttranslational modification, which can affect binding of nanobodies, or the CD39 transfected HEK cells and Tregs exhibit different sequences and therefore a slightly different conformation. Since the expression plasmid for mouse CD39 was not newly generated for this study, we traced down its origin, sequenced the CD39 encoding region (termed CD39var in the following) and compared the translated amino acid sequence to the one from the reference sequence for CD39 (UniProtKB: P55772, termed CD39ref in the following). This search revealed that CD39var is identical with a CD39 variant under the GenBank accession number AAH11278.1. The sequence for this protein originates from a murine mammary tumor, which was induce by infecting mice with the mouse mammary tumor virus (MMTV). When aligned with the CD39ref, there was a two amino acids difference at positions 158 (S158G) and 302 (K302E) (**Figure 5.1**). To further investigate this, CD39ref stably transfected HEK293-T cells were generated, and the binding of two selected clones (2-1 and 13-2) to CD39ref was probed and their specificity to CD39ref is consistent with their specificity to B6 Tregs (**Figure 5.2**). Therefore, it is likely that the lack of binding of mouse CD39 nanobodies to Tregs is due to the sequence and potentially structural difference of both CD39 variants.

Different from B6 mice which were used for screening in this study, CD39var originates from the Czech II mouse strain (Strausberg et al. 2002). As shown in **Figure 5.1**, the mutation at S158 is a semi-conservative mutation, which means it is a single nucleotide polymorphism (SNP) between two mouse strains. The conservative mutation at K302, might be associated cancer-based mutagenesis, however, this cannot be verified to date. Since MMTV has been found to randomly induce single-nucleotide variants (SNV) in mouse tumor models and tumor cell line (Rennhack et al. 2019) (Schrörs et al. 2020), K302E could have also been caused by MMTV infection. Although these two mutations lead to a failure in generating CD39ref-specific nanobodies, one can develop a very interesting perspective from it: mutations in cell surface proteins that are developing during tumorigenesis could be used as specific targets for immunotherapy of tumors. From the example of CD39 one

could see that a two amino acid difference can decide over binding or not-binding. A treatment approach with the tumor specific anti-CD39var nanobodies, modified to kill tumor cells e.g. by adding an IgG-Fc for natural killer cell (NK) or complement system activation (Scott et al. 2012), one would selectively target and kill tumor cells, whereas other cells expressing the unmutated variant of CD39 (CD39ref), such as Tregs and NK cells (Moesta et al. 2020), would be protected from depletion. Besides, the CD39var inhibitory nanobody clone 2-1 identified in this study could exert anti-tumor effects by reducing the tumor-induced inhibition of CD4 and CD8 T cell proliferation and enhancing NK- and cytotoxic effector CD8 T cell-mediated cytotoxicity (Bastid et al. 2015).

```
CD39ref       MEDIKDSKVKRFCSKNILIILGFTSILAVIALIAVGLTQNKPLPENVKYGIVLDAGSSHT      60
CD39var       MEDIKDSKVKRFCSKNILIILGFTSILAVIALIAVGLTQNKPLPENVKYGIVLDAGSSHT      60
              ************************************************************

CD39ref       NLYIYKWPAEKENDTGVVQQLEECQVKGPGISKYAQKTDEIGAYLAECMELSTELIPTSK      120
CD39var       NLYIYKWPAEKENDTGVVQQLEECQVKGPGISKYAQKTDEIGAYLAECMELSTELIPTSK      120
              ************************************************************

CD39ref       HHQTPVYLGATAGMRLLRMESEQSADEVLAAVSTSLKSYPFDFQGAKIITGQEEGAYGWI      180
CD39var       HHQTPVYLGATAGMRLLRMESEQSADEVLAAVSTSLKGYPFDFQGAKIITGQEEGAYGWI      180
              ************************************.***********************

CD39ref       TINYLLGRFTQEQSWLSLISDSQKQETFGALDLGGASTQITFVPQNSTIESPENSLQFRL      240
CD39var       TINYLLGRFTQEQSWLSLISDSQKQETFGALDLGGASTQITFVPQNSTIESPENSLQFRL      240
              ************************************************************

CD39ref       YGEDYTVYTHSFLCYGKDQALWQKLAKDIQVSSGGVLKDPCFNPGYEKVVNVSELYGTPC      300
CD39var       YGEDYTVYTHSFLCYGKDQALWQKLAKDIQVSSGGVLKDPCFNPGYEKVVNVSELYGTPC      300
              ************************************************************

CD39ref       TKRFEKKLPFDQFRIQGTGDYEQCHQSILELFNNSHCPYSQCAFNGVFLPPLHGSFGAFS      360
CD39var       TERFEKKLPFDQFRIQGTGDYEQCHQSILELFNNSHCPYSQCAFNGVFLPPLHGSFGAFS      360
              *:************************************************************

CD39ref       AFYFVMDFFKKVAKNSVISQEKMTEITKNFCSKSWEETKTSYPSVKEKYLSEYCFSGAYI      420
CD39var       AFYFVMDFFKKVAKNSVISQEKMTEITKNFCSKSWEETKTSYPSVKEKYLSEYCFSGAYI      420
              ************************************************************

CD39ref       LSLLQGYNFTDSSWEQIHFMGKIKDSNAGWTLGYMLNLTNMIPAEQPLSPPLPHSTYIGL      480
CD39var       LSLLQGYNFTDSSWEQIHFMGKIKDSNAGWTLGYMLNLTNMIPAEQPLSPPLPHSTYIGL      480
              ************************************************************

CD39ref       MVLFSLLLVAVAITGLFIYSKPSYFWKEAV       510
CD39var       MVLFSLLLVAVAITGLFIYSKPSYFWKEAV       510
              ******************************
```

Figure 5.1: CD39var vs CD39ref amino acid sequences. The sequences of CD39var and CD39ref were aligned using Clustal Omega. The symbols (*), (.) and (:) below the protein sequences denote conserved sequence, semi-conservative mutation and conservative mutation respectively.

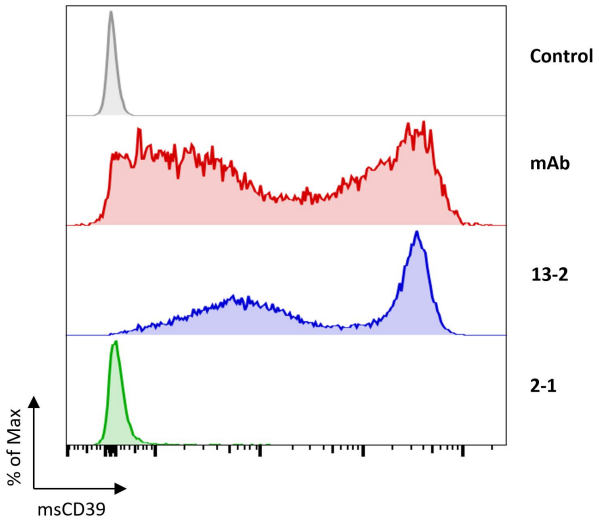

Figure 5.2: Some of the selected msCD39 specific nanobodies cannot bind to CD39ref. HEK293-T cells were transfected with CD39ref plasmid and stained with a fluorochrome conjugated anti-CD39 mAb or clones 2-1 and 13-2 as rb-Fc fusion protein in combination with a fluorochrome conjugated anti-rb IgG secondary antibody.

5.3 Antagonistic properties of the nanobodies and their further use

Several nanobodies identified in this study (especially fam 11 specific for human CD39, fam 2 specific for mouse CD39, fam 18.1 and fam 20 specific for mouse CD73 and all human CD73 specific nanobodies) showed inhibitory effects regarding the enzymatic activity of their corresponding target. To date, several small molecule compounds and mAbs targeting CD39 and CD73 have been generated and characterized. Small molecule inhibitors of CD39 mainly are comprised of nucleotide analogs (such as 6-N,N-diethyl-D-β,γ-dibromomethylene-ATP-trisodium salt (ARL-67156)), sulfonate dyes and anthraquinones (such as Evans Blue and Reactive Blue 2) and polyoxotungstate (such as sodium polyoxotungstate (POM-1)), while small molecule of CD73 inhibitors are mainly derived from nucleosides (Jeffrey et al. 2020). However, except for several CD73 inhibitors (Bowman et al. 2019), the inhibitors mentioned above either are non-selective inhibitors or show weak inhibitory activity or have significant off-target activity (Spatola et al. 2020) (Jeffrey et al. 2020). Apart from small molecule inhibitor, mAbs against CD39 and CD73 were developed and studied by several research groups in the past years. Tang et al. performed a global immuno-oncology landscape in 2018, 4 and 16 active agents against CD39 and CD73 were under investigation, respectively (Tang et al. 2018). However, compared to small molecule and mAb, nanobodies have several advantages. They can bind to

different epitopes compared to mAb (Jovčevska and Muyldermans 2020), they are more stable in harsh conditions e.g. temperature and pH, and they can easier penetrate into tissues due to their smaller size and the lack of an an Fc part (Liu et al. 2021). Nanobodies are as specific to their targets as mAbs and off-target related side effects are much less common among therapeutic nanobodies and mAbs when compared to small molecule inhibitors (Menzel et al. 2018). In addition, the size of nanobodies is tunable by gene engineering, which provide the possibility to conjugate agents like drugs and radioisotopes for disease diagnosis and therapy (Wesolowski et al. 2009) (Liu et al. 2021).

Specific inhibitors generated in this study can potentially be applied in disease settings, where CD39 and CD73 are either overexpressed or functionally relevant in the disease pathology. CD39 and CD73 are involved in many diseases, such as AIDS (Nikolova et al. 2011), allergic asthma (Wang et al. 2013), ischemic diseases (Roberts et al. 2013) and chronic inflammatory disorders (Longhi et al. 2017). Further, many types of cancer have been reported to exhibit increased expression of CD39 and CD73 and blocking either CD39 or CD73 enzymatic activity demonstrates significant anti-tumor effects (Bastid et al. 2013) (Chen et al. 2019). To date, several CD39 and CD73 specific mAbs inhibitors have entered clinical trials: CD39 inhibitors (TTX-030, SRF617 and IPH5201) are in Phase 1 to Phase 1/1b stages, and CD73 inhibitors (MEDI9447, BMS-986179, CPI-006, NZV930, GS-1423 and TJ004309) are in Phase 1 to Phase 2 stages (**Table 5.2**). Preliminary data of these clinical trials indicate that targeting CD39 and CD73 in cancer can be beneficial for the outcome. However, none of the clinical trials focus on tumors in CNS. Although it remains challenging to deliver nanobodies to the brain, but Jovčevska reported several potential ways for nanobodies to cross the BBB (Jovčevska and Muyldermans 2020). Therefore, except for the studied tumors, our nanobody candidates also have the possibility to be used for targeting tumor cells in CNS.

Table 5.2 Summary of clinical trials of anti-CD39 and anti-CD73 mAbs inhibitors on cancer

(informations are collected on 2021.08.05 from clinicaltrials.gov)

Agent	NCT Number	Stage	Status	Conditions
anti-CD39 mAb inhibitors				
TTX-030	NCT03884556	Phase 1/1b	Recruiting	Solid Tumor; Lymphoma
	NCT04306900	Phase 1/1b	Recruiting	Solid Tumor, Adult
SRF617	NCT04336098	Phase 1	Recruiting	Advanced Solid Tumor
IPH5201	NCT04261075	Phase 1	Recruiting	Advanced Solid Tumors
anti-CD73 mAb inhibitors				
MEDI9447	NCT03736473	Phase 1	Completed	Advanced Solid Malignancies
	NCT02503774	Phase 1	Active, not recruiting	Solid Tumors
	NCT03611556	Phase 1b/2	Recruiting	Carcinoma; Metastatic Pancreatic Adenocarcinoma
	NCT03381274	Phase 1b/2	Active, not recruiting	Carcinoma, Non-Small-Cell Lung Cancer (NSCLC)
	NCT03773666	Phase 1	Active, not recruiting	Muscle Invasive Bladder Cancer
	NCT03616886	Phase 1/2	Recruiting	Triple Negative Breast Cancer
	NCT03267589	Phase 2	Recruiting	Ovarian Cancer
	NCT04089553	Phase 2	Active, not recruiting	Prostate Cancer; Metastatic Castration-Resistant Prostate Cancer (mCRPC)
	NCT04668300	Phase 2	Recruiting	Angiosarcoma; Dedifferentiated Liposarcoma; Osteosarcoma
	NCT03875573	Phase 2	Active, not recruiting	Luminal B
	NCT03819465	Phase 1b	Active, not recruiting	Metastatic NSCLC
	NCT03833440	Phase 2	Recruiting	NSCLC
	NCT04068610	Phase 1b/2	Active, not recruiting	Metastatic Microsatellite-stable Colorectal Cancer (CRC)
	NCT04940286	Phase 2	Not yet recruiting	Pancreatic Adenocarcinoma
	NCT03822351	Phase 2	Active, not recruiting	NSCLC
	NCT03742102	Phase 1b/2	Recruiting	Triple Negative Breast Neoplasms
	NCT02740985	Phase 1	Active, not recruiting	Advanced Solid Malignancies; NSCLC; mCRPC; CRC
	NCT03334617	Phase 2	Recruiting	NSCLC
BMS-986179	NCT02754141	Phase 1/2a	Active, not recruiting	Malignant Solid Tumor
CPI-006	NCT03454451	Phase 1/1b	Recruiting	Advanced solid malignancies
NZV930	NCT03549000	Phase 1/1b	Recruiting	Advanced solid malignancies
	NCT04237649	Phase 1/1b	Recruiting	Solid Tumors
GS-1423	NCT03954704	Phase 1a/1b	Terminated	Advanced Solid Tumors
TJ004309	NCT04322006	Phase 1/2	Recruiting	Advanced Solid Tumor
	NCT03835949	Phase 1	Active, not recruiting	Solid Tumor; Metastatic Cancer

In this study, all characterizations of nanobodies were performed with HEK293-6E supernatant, which means the nanobody concentration is low, but some clones (fam 11 to human CD39, fam 2 to mouse CD39, fam 18.1 and fam 20 to mouse CD73 and

all human CD73 binders) have shown strong inhibitory effects. Therefore, inhibitory nanobodies identified in this study are of great potential and interest. However, further experiments are still needed to expand knowledge of nanobody candidates, including but not limit to affinity assays and half maximal inhibitory concentration (IC_{50}) assays to compare with existing CD39 and CD73 inhibitory small molecule inhibitors and mAb (Jeffrey et al. 2020). This will allow to identify the 2-3 top candidates for each target that exhibit i) specific binding to their targets, ii) binding with high affinity, iii) maxium possible antagonistic properties regarding the enzymatic activity of their targets and finally iv) good production yield and storage stability. Once these top candidates have been identified the therapeutic potential of mouse specific nanobodies could be evaluated in disease models followed by clinical trials with human specific nanobodies.

6. Summary

CD39 and CD73 are the two key ecto-enzymes in the process of converting pro-inflammatory ATP into anti-inflammatory adenosine. The enzymatic activity of both ecto-enzymes modulates the course inflammation associated diseases, including cancer. Compared to conventional antibodies, nanobodies are much smaller, exhibit better tissue penetration and are well suited for targeting the active site of enzymes.

In this thesis, nanobodies against mouse and human CD39 and CD73 were successfully generated. After screening on transfected HEK cells, 11 and 9 families of specific binders to CD39 and CD73 were identified, respectively. Among 11 CD39 specific families, four families were specific for mouse CD39, six families were specific to human CD39, and one family was cross-reactive to mouse and human CD39. For CD73, three mouse CD73 and three human CD73 specific families and three cross-reactive families were identified. The specificity to primary mouse and human immune cells was also evaluated. Here, human CD39, mouse and human CD73 specific nanobodies could showed propper bind to their specific target on primary cells, whereas most mouse CD39 specific nanobodies (except for fam3 and fam13) failed to bind to primary mouse cells.

The capacity of selected nanobodies towards modulating the enzymatic activity of their target was further evaluated. For human CD39-specific nanobodies, fam11 and fam15 showed strong inhibition of CD39 enzymatic activity, while fam17 and fam19 only slightly inhibit ATP degradation. For mouse CD39 specific nanobodies, fam2 exhibited CD39-inhibiting capacity, while fam10 and fam16 showed only minor inhibitory effect. The cross-reactive fam3 could slightly inhibit mouse CD39 but had no impact on human CD39 activity.

Among all CD73 specific nanobodies, four mouse CD73 specific and five human CD73 specific nanobodies were evaluated towards their CD73-modulating capacity. Regarding mouse CD73 specific nanobodies, clone 18-6 showed proper inhibition of mouse CD73 activity, whereas clone 20-1 showed moderate inhibitory capacity. All five human CD73 binders showed moderate inhibition of CD73 activity in the AMP degradation assay.

In summary, mouse and human CD39 and CD73 specific nanobodies were successfully generated in this project and promising antagonists have been identified for each target. These newly developed nanobodies could serve as new generation of

CD39/CD73 inhibiting drugs to be tested in preclinical mouse models and, after positive results, also in clinical trials e.g. as new anti-tumor drugs.

Zusammenfassung

CD39 und CD73 sind die beiden Schlüssel-Ektoenzyme bei der Umwandlung von proinflammatorischem ATP in entzündungshemmendes Adenosin. Die enzymatische Aktivität beider Ektoenzyme moduliert den Verlauf entzündungsbedingter Erkrankungen, einschließlich Krebs. Im Vergleich zu herkömmlichen Antikörpern sind Nanobodies viel kleiner, weisen eine bessere Gewebepenetration auf und eignen sich gut, um das aktive Zentrum von Enzymen zu blockieren.

In dieser Arbeit wurden Nanobodies gegen Maus- und Human-CD39 und CD73 generiert. Nach dem Screening auf transfizierten HEK-Zellen wurden 11 bzw. 9 Familien spezifischer Binder für CD39 bzw. CD73 identifiziert. Von den 11 CD39-spezifischen Familien waren vier Familien spezifisch für Maus-CD39, sechs Familien waren spezifisch für Human-CD39 und eine Familie war kreuzreaktiv für Maus- und Human-CD39. Für CD73 wurden drei Maus-CD73- und drei Human-CD73-spezifische Familien sowie drei kreuzreaktive Familien identifiziert. Die Spezifität für primäre Maus- und Human-Immunzellen wurde ebenfalls untersucht. Hier konnten humane CD39-, Maus- und humane CD73-spezifische Nanobodies eine gute Bindung an ihr spezifisches Ziel auf primären Zellen vorweisen, wo hingegen die meisten Maus-CD39-spezifischen Nanobodies (außer fam3 und fam13) nicht an primäre Mauszellen binden konnten.

Die Fähigkeit ausgewählter Nanobodies zur Modulation der enzymatischen Aktivität ihres Targets wurde weiter untersucht. Für humane CD39-spezifische Nanobodies zeigten fam11 und fam15 eine starke Hemmung der enzymatischen Aktivität von CD39, während fam17 und fam19 nur geringfügig den ATP-Abbau hemmen. Bei Maus-CD39-spezifischen Nanobodies zeigte fam2 eine solide Inhibierung der CD39 Enzymaktivität, während fam10 und fam16 nur eine geringe inhibitorische Wirkung zeigten. Die Maus/Mensch kreuzreaktive Familie fam3 konnte die Aktivität von Maus-CD39 leicht hemmen, hatte jedoch keinen Einfluss auf die menschliche CD39 Aktivität.

Von allen CD73-spezifischen Nanobodies wurden vier CD73-spezifische Maus- und fünf Human-CD73-spezifische Nanobodies hinsichtlich ihrer CD73-modulierenden Kapazität bewertet. Unter den Maus-CD73-spezifische Nanobodies zeigte Klon 18-6 eine gute Hemmung der Maus-CD73 Enzymaktivität, während Klon 20-1 eine mäßige

Hemmungskapazität aufwies. Alle fünf humanen CD73 Binder zeigten eine moderate Hemmung der CD73-Aktivität im AMP-Abbauassay.

Zusammenfassend lässt sich sagen, dass in diesem Projekt erfolgreich CD39- und CD73-spezifische Nanobodies gegen Maus und Mensch CD39/CD73 erzeugt wurden und für jedes Zielmolekül vielversprechende Antagonisten identifiziert wurden. Diese neu entwickelten Nanobodies könnten als neue Generation von CD39/CD73-hemmenden Medikamenten dienen, die in präklinischen Mausmodellen und nach positiven Ergebnissen auch in klinischen Studien, z.B. als neue Anti-Tumor-Medikamente getestet werden.

7. Appendix:

7.1 Sequence alignment of alpaca, mouse and human CD39

```
AlpacaCD39      ------------MEDRRESELKRFCSRNILSILGFSSIIAVIALLALGLVQNKPLPENVK   48
mouseCD39       ------------MEDIKDSKVKRFCSKNILIILGFTSILAVIALIAVGLTQNKPLPENVK   48
humanCD39       MGREELFLTFSFSSGFQESNVKTFCSKNILAILGFSSIIAVIALLAVGLTQNKALPENVK   60
                             .. ::*::* ***:*** ****:**:*****:*:**.*** ******

AlpacaCD39      FGIVLDAGSSHTSLYIYQWPAEKENDTGMVSQVEECKVQGPGIANHVQKLSEIDVYLAAC   108
mouseCD39       YGIVLDAGSSHTNLYIYKWPAEKENDTGVVQQLEECQVKGPGISKYAQKTDEIGAYLAEC   108
humanCD39       YGIVLDAGSSHTSLYIYKWPAEKENDTGVVHQVEECRVKGPGISKFVQKVNEIGIYLTDC   120
                :**********.****:**********:* *:***:*:****::..** .**. **: *

AlpacaCD39      MERAKVVIPAPQHTETPVYLGATAGMRLLRMKNGYLASKILAVVTSSISNYPFDFQGARI   168
mouseCD39       MELSTELIPTSKHHQTPVYLGATAGMRLLRMESEQSADEVLAAVSTSLKGYPFDFQGAKI   168
humanCD39       MERAREVIPRSQHQETPVYLGATAGMRLLRMESEELADRVLDVVERSLSNYPFDFQGARI   180
                ** :  :**  :* :****************:.   *..:* .*  *:..********:*

AlpacaCD39      ITGQEEGAYGWITTNYLLGRFTQKSSWFNLKPTGGEPQETYGALDLGGASTQITFVPKDK   228
mouseCD39       ITGQEEGAYGWITINYLLGRFTQEQSWLSLIS-DSQKQETFGALDLGGASTQITFVPQNS   227
humanCD39       ITGQEEGAYGWITINYLLGKFSQKTRWFSIVPYETNNQETFGALDLGGASTQVTFVPQNQ   240
                ************* *****:*:*:  *:.:     : ***:***********:****::.

AlpacaCD39      TMESPDDTLHFRLYGRNYSVYTHSFLCYGKDQALLQKLAKDVRNT-DGTISDPCFHPGYQ   287
mouseCD39       TIESPENSLQFRLYGEDYTVYTHSFLCYGKDQALWQKLAKDIQVSSGGVLKDPCFNPGYE   287
humanCD39       TIESPDNALQFRLYGKDYNVYTHSFLCYGKDQALWQKLAKDIQVASNEILRDPCFHPGYK   300
                *:***:::*:*****.:*.*************** ******:: : .  : ****:***:

AlpacaCD39      RKMVLADLYESPCTRKFETFLQFDEIIIQGTGNYQQCQQSILQLFNTSYCPYSHCAFDGI   347
mouseCD39       KVVNVSELYGTPCTERFEKKLPFDQFRIQGTGDYEQCHQSILELFNNSHCPYSQCAFNGV   347
humanCD39       KVVNVSDLYKTPCTKRFEMTLPFQQFEIQGIGNYQQCHQSILELFNTSYCPYSQCAFNGI   360
                : : :::** :***.:**  * *::: *** *:*:**:****:***.*:****:***:*:

AlpacaCD39      FLPPVQGDFGAFSAFYYVMEFLNLTSK-EHLSPKKMTDMMEEFCSQPWEKLQVYFSDVKE   406
mouseCD39       FLPPLHGSFGAFSAFYFVMDFFKKVAKNSVISQEKMTEITKNFCSKSWEETKTSYPSVKE   407
humanCD39       FLPPLQGDFGAFSAFYFVMKFLNLTS--EKVSQEKVTEMMKKFCAQPWEEIKTSYAGVKE   418
                ****::*.********:**.*:: .:  . :* :*:*:: ::**:: **: :. : .***

AlpacaCD39      NYLSEYCFSGTYILTLLLNGYHFTAETWKNIHFMGKVRSTSVGWTLGYMLNLTNMIPAEE   466
mouseCD39       KYLSEYCFSGAYILSL-LQGYNFTDSSWEQIHFMGKIKDSNAGWTLGYMLNLTNMIPAEQ   466
humanCD39       KYLSEYCFSGTYILSLLLQGYHFTADSWEHIHFIGKIQGSDAGWTLGYMLNLTNMIPAEQ   478
                :*********:***:* *:**:** .:*::***:**::.:..*****************:

AlpacaCD39      PPSAPLPHSTYVFLMVFFSLILVIVVLLCIFAFHKPSFFWEDVV   510
mouseCD39       PLSPPLPHSTYIGLMVLFSLLLVAVAITGLFIYSKPSYFWKEAV   510
humanCD39       PLSTPLSHSTYVFLMVLFSLVLFTVAIIGLLIFHKPSYFWKDMV   522
                * * ** ****: ***:***:*. *.:  :: : ***:**:: *
```

7.2 Sequence alignment of alpaca, mouse and human CD73

```
AlpacaCD73      MRPPAARVLALRLLALWA--LLWPAAGAWELTVLHTNDVHSRLEQTSEDSGKCVNASRCV   58
mouseCD73       MRPAAAKVPKWLLLALSALLPQWPAASAWELTILHTNDVHSRLEQTSDDSTKCLNASLCV   60
humanCD73       MCPRAARAPATLLLALGA--VLWPAAGAWELTILHTNDVHSRLEQTSEDSSKCVNASRCM   58
                * * **:.    **** *    ****.*****:**************:** **:*** *:

AlpacaCD73      GGVARLATKVRQIRRAEPHVLLLDAGDQYQGTIWFTVYKGAEVAHFMNALSYDAMALGNH   118
mouseCD73       GGVARLFTKVQQIRKEEPNVLFLDAGDQYQGTIWFTVYKGLEVAHFMNILGYDAMALGNH   120
humanCD73       GGVARLFTKVQQIRRAEPNVLLLDAGDQYQGTIWFTVYKGAEVAHFMNALRYDAMALGNH   118
                ****** ***:***: **:**:****************** ******* * *********

AlpacaCD73      EFDNGVEGLIEPLLKEAKFPILSANIKAKGPLASRISGLYSPYKILRVGDEVVGIVGYTS   178
mouseCD73       EFDNGVEGLIDPLLRNVKFPILSANIKARGPLAHQISGLFLPSKVLSVGGEVVGIVGYTS   180
humanCD73       EFDNGVEGLIEPLLKEAKFPILSANIKAKGPLASQISGLYLPYKVLPVGDEVVGIVGYTS   178
                **********:***::.**********:**** :****: * *:* **.**********

AlpacaCD73      KETPFLSNPGTNLVFEDEIAALQPEVDKLQTLNVNKIIALGHSGFEMDKLIAQKVKGVDV   238
mouseCD73       KETPFLSNPGTNLVFEDEISALQPEVDKLKTLNVNKIIALGHSGFEMDKLIAQKVRGVDI   240
humanCD73       KETPFLSNPGTNLVFEDEITALQPEVDKLKTLNVNKIIALGHSGFEMDKLIAQKVRGVDV   238
                ********************:*********:**************************:***:

AlpacaCD73      VVGGHSNTFLYTGNPPSKEVPAGQYPFIVTSDDGRKVPVVQAYAFGKYLGYLKVEFDEKG   298
mouseCD73       VVGGHSNTFLYTGNPPSKEVPAGKYPFIVTADDGRQVPVVQAYAFGKYLGYLKVEFDDKG   300
humanCD73       VVGGHSNTFLYTGNPPSKEVPAGKYPFIVTSDDGRKVPVVQAYAFGKYLGYLKIEFDERG   298
                ************************:*******:****:******************:***::*

AlpacaCD73      NVITSHGNPILLNSSIPEDPSIKADINKWRIKLDNYSTQELGRTIVYLDGTTQSCRFREC   358
mouseCD73       NVITSYGNPILLNSSIPEDATIKADINQWRIKLDNYSTQELGRTIVYLDGSTQTCRFREC   360
humanCD73       NVISSHGNPILLNSSIPEDPSIKADINKWRIKLDNYSTQELGKTIVYLDGSSQSCRFREC   358
                ***:*:************** :******:**************:*******::*:*******

AlpacaCD73      NMGNLICDAMINNNLRHTDEMSWNHVSMCIMNGGGIRSPIDERNNGTITWENLAAVLPFG   418
mouseCD73       NMGNLICDAMINNNLRHPDEMFWNHVSMCIVNGGGIRSPIDEKNNGTITWENLAAVLPFG   420
humanCD73       NMGNLICDAMINNNLRHTDEMFWNHVSMCILNGGGIRSPIDERNNGTITWENLAAVLPFG   418
                ****************** *** ********:***********:******************

AlpacaCD73      GTFDLVQLKGSTLKKAFEHSVYRYGQSTGEFLQVGGIHVVYDLSRKPGDRVVKLDVLCTQ   478
mouseCD73       GTFDLVQLKGSTLKKAFEHSVHRYGQSTGEFLQVGGIHVVYDINRKPWNRVVQLEVLCTK   480
humanCD73       GTFDLVQLKGSTLKKAFEHSVHRYGQSTGEFLQVGGIHVVYDLSRKPGDRVVKLDVLCTK   478
                **********************:**********************:.*** :***:*:*****:

AlpacaCD73      CRVPSYEPLRMDEVYKVILTSFLANGGDGFQMIKDEALKHDSGDQDISVVSGYILKMRVV   538
mouseCD73       CRVPIYEPLEMDKVYKVTLPSYLANGGDGFQMIKDELLKHDSGDQDISVVSEYISKMKVV   540
humanCD73       CRVPSYDPLKMDEVYKVILPNFLANGGDGFQMIKDELLRHDSGDQDINVVSTYISKMKVI   538
                **** *:**.**:**** * .:*************** *:********.*** ** **:*:

AlpacaCD73      YPAVEGRIQFSAGSHCHGSFSLIFLTVLAVIIVLYQ   574
mouseCD73       YPAVEGRIKFSAASHYQGSFPLVILSFWAMILILYQ   576
humanCD73       YPAVEGRIKFSTGSHCHGSFSLIFLSLWAVIFVLYQ   574
                ********:**:.** :*** *::*:. *:*::***
```

8. Abbreviation

AC	adenylyl cyclase
ACR	apyrase conserved region
ADP	adenosine diphosphate
AMP	adenosine monophosphate
ATP	adenosine triphosphate
BBB	blood brain barrier
cAMP	cyclic adenosine monophosphate
CCL2	C-C motif chemokine ligand 2
CD39var	mouse CD39 used for immunization and characterization in this study
CD39ref	reference sequence for mouse CD39
CDR	complementary determining regions
CH	constant domains of heavy chain
CL	constant domains of light chain
CNS	central nervous system
COPD	chronic obstructive pulmonary disease
CRC	colorectal cancer
DAMP	damage-associated molecular patterns
eAMP	etheno-AMP
ENPP	ecto-nucleotide pyrophosphate phosphodiesterase
ENTPDase	ectonucleoside triphosphate diphosphohydrolase
Fab	antigen-binding fragment
FACS	fluorescence-activated cell sorting
FR	framework regions
Fv	variable fragment
GPCR	G-protein-coupled receptor
GPI	glycosyl-phosphatidyl inositol
GvHD	graft-versus-host disease
HCAb	heavy-chain antibody
HEK	human embryonic kidney
HPLC	high-performance liquid chromatography

IBD	inflammatory bowel disease
IC_{50}	half maximal inhibitory concentration
Ig	immunoglobulin
Ig-NAR	immunoglobulin new antigen receptor
IL-6	interleukin 6
IPF	idiopathic pulmonary fibrosis
mAb	monoclonal antibody
mCRPC	castration-resistant prostate cancer
MMTV	mouse mammary tumor virus
Nb	nanobody
NF-kB	nuclear factor kappa-light-chain-enhancer of activated B cells
NK	natural killer cell
NLRP3	NOD-, LRR- and pyrin domain-containing protein 3
NSCLC	non-small-cell lung cancer
P2XR	P2X receptor
P2YR	P2Y receptor
PBMC	peripheral blood mononuclear cell
PCR	polymerase chain reaction
PEG	polyethylene glycol
Pi-PLC	phosphoinositide phospholipase C
RT	reverse translation
SNP	single nucleotide polymorphism
SNV	single-nucleotide variants
TNF	tumor necrosis factor
UDP	uridine diphosphate
UTP	uridine triphosphate
VEGF	vascular endothelial growth factor
VH	variable domain of heavy chain
VHH	variable domain of heavy-chain antibody
VL	variable domain of light chain

9. Reference

Ackaert C, Smiejkowska N, Xavier C, Sterckx YGJ, Denies S, Stijlemans B, Elkrim Y, Devoogdt N, Caveliers V, Lahoutte T, Muyldermans S, Breckpot K, Keyaerts M. Immunogenicity Risk Profile of Nanobodies. Front Immunol. 2021;12:632687.

Adinolfi E, Giuliani AL, De Marchi E, Pegoraro A, Orioli E, Di Virgilio F. Shieh. Biochem Pharmacol. 2018;151:234–44.

Allard D, Allard B, Gaudreau P-O, Chrobak P, Stagg J. CD73–adenosine: a next-generation target in immuno-oncology. Immunotherapy. 2016;8(2):145–63.

Allard D, Allard B, Stagg J. On the mechanism of anti-CD39 immune checkpoint therapy. J Immunother Cancer. BMJ Specialist Journals; 2020;8(1):e000186.

Bastid J, Cottalorda-Regairaz A, Alberici G, Bonnefoy N, Eliaou J-F, Bensussan A. ENTPD1/CD39 is a promising therapeutic target in oncology. Oncogene. 2013;32(14):1743–51.

Bastid J, Regairaz A, Bonnefoy N, Déjou C, Giustiniani J, Laheurte C, Cochaud S, Laprevotte E, Funck-Brentano E, Hemon P, Gros L, Bec N, Larroque C, Alberici G, Bensussan A, Eliaou J-F. Inhibition of CD39 enzymatic function at the surface of tumor cells alleviates their immunosuppressive activity. Cancer Immunol Res. 2015;3(3):254–65.

von Behring E, Kitasato S. [The mechanism of diphtheria immunity and tetanus immunity in animals]. Mol Immunol. 1890;28(12):1317, 1319–20.

Bhattarai S, Pippel J, Meyer A, Freundlieb M, Schmies C, Abdelrahman A, Fiene A, Lee S-Y, Zimmermann H, El-Tayeb A, Yegutkin GG, Sträter N, Müller CE. X-Ray Co-Crystal Structure Guides the Way to Subnanomolar Competitive Ecto-5′-Nucleotidase (CD73) Inhibitors for Cancer Immunotherapy. Adv Ther. 2019;2(10):1900075.

Bonnefoy N, Bastid J, Alberici G, Bensussan A, Eliaou J-F. CD39: A complementary target to immune checkpoints to counteract tumor-mediated immunosuppression. OncoImmunology. 2015;4(5):e1003015.

Bono MR, Fernández D, Flores-Santibáñez F, Rosemblatt M, Sauma D. CD73 and CD39 ectonucleotidases in T cell differentiation: Beyond immunosuppression. FEBS Lett. 2015;589(22):3454–60.

Borea PA, Varani K, Vincenzi F, Baraldi PG, Tabrizi MA, Merighi S, Gessi S. The A3 Adenosine Receptor: History and Perspectives. Pharmacol Rev. 2015;67(1):74–102.

Bours MJL, Swennen ELR, Di Virgilio F, Cronstein BN, Dagnelie PC. Adenosine 5′-triphosphate and adenosine as endogenous signaling molecules in immunity and inflammation. Pharmacol Ther. 2006;112(2):358–404.

Bowman CE, da Silva RG, Pham A, Young SW. An Exceptionally Potent Inhibitor of Human CD73. Biochemistry. 2019;58(31):3331–4.

Burnstock G. Purinergic Nerves. Pharmacol Rev. 1972;24(3):509–81.

Burnstock G. Purine and purinergic receptors. Brain Neurosci Adv.

2018;2:2398212818817494.

Chen J-F, Eltzschig HK, Fredholm BB. Adenosine receptors as drug targets — what are the challenges? Nat Rev Drug Discov. 2013;12(4):265–86.

Chen S, Wainwright DA, Wu JD, Wan Y, Matei DE, Zhang Y, Zhang B. CD73: an emerging checkpoint for cancer immunotherapy. Immunotherapy. 2019;11(11):983–97.

Chen Y, Corriden R, Inoue Y, Yip L, Hashiguchi N, Zinkernagel A, Nizet V, Insel PA, Junger WG. ATP release guides neutrophil chemotaxis via P2Y2 and A3 receptors. Science. 2006;314(5806):1792–5.

Clackson T, Hoogenboom HR, Griffiths AD, Winter G. Making antibody fragments using phage display libraries. Nature. 1991;352(6336):624.

Cortez-Retamozo V, Backmann N, Senter PD, Wernery U, Baetselier PD, Muyldermans S, Revets H. Efficient Cancer Therapy with a Nanobody-Based Conjugate. Cancer Res. American Association for Cancer Research; 2004;64(8):2853–7.

Desmyter A, Transue TR, Ghahroudi MA, Thi M-HD, Poortmans F, Hamers R, Muyldermans S, Wyns L. Crystal structure of a camel single-domain V H antibody fragment in complex with lysozyme. Nat Struct Biol. 1996;3(9):803.

Di Virgilio F, Dal Ben D, Sarti AC, Giuliani AL, Falzoni S. The P2X7 Receptor in Infection and Inflammation. Immunity. 2017;47(1):15–31.

Eckle T, Koeppen M, Eltzschig HK. Role of Extracellular Adenosine in Acute Lung Injury. Physiology. 2009;24(5):298–306.

Eden T, Menzel S, Wesolowski J, Bergmann P, Nissen M, Dubberke G, Seyfried F, Albrecht B, Haag F, Koch-Nolte F. A cDNA Immunization Strategy to Generate Nanobodies against Membrane Proteins in Native Conformation. Front Immunol. 2018;8.

Eltzschig HK, Sitkovsky MV, Robson SC. Purinergic Signaling during Inflammation. N Engl J Med. 2012;367(24):2322–33.

Falzoni Simonetta, Donvito Giovanna, Di Virgilio Francesco. Detecting adenosine triphosphate in the pericellular space. Interface Focus. 2013;3(3):20120101.

Figliuolo VR, Savio LEB, Safya H, Nanini H, Bernardazzi C, Abalo A, de Souza HSP, Kanellopoulos J, Bobé P, Coutinho CMLM, Coutinho-Silva R. P2X7 receptor promotes intestinal inflammation in chemically induced colitis and triggers death of mucosal regulatory T cells. Biochim Biophys Acta Mol Basis Dis. 2017;1863(6):1183–94.

Flajnik MF, Deschacht N, Muyldermans S. A case of convergence: why did a simple alternative to canonical antibodies arise in sharks and camels? PLoS Biol. 2011;9(8):e1001120.

Forrester T. An estimate of adenosine triphosphate release into the venous effluent from exercising human forearm muscle. J Physiol. 1972;224(3):611–28.

Ghahroudi MA, Desmyter A, Wyns L, Hamers R, Muyldermans S. Selection and identification of single domain antibody fragments from camel heavy-chain antibodies. FEBS Lett. 1997;414(3):521–6.

Ghalamfarsa G, Kazemi MH, Raoofi Mohseni S, Masjedi A, Hojjat-Farsangi M, Azizi G, Yousefi M, Jadidi-Niaragh F. CD73 as a potential opportunity for cancer immunotherapy. Expert Opin Ther Targets. 2019;23(2):127–42.

Goldman ER, Liu JL, Zabetakis D, Anderson GP. Enhancing Stability of Camelid and Shark Single Domain Antibodies: An Overview. Front Immunol. 2017;8.

Govaert J, Pellis M, Deschacht N, Vincke C, Conrath K, Muyldermans S, Saerens D. Dual Beneficial Effect of Interloop Disulfide Bond for Single Domain Antibody Fragments. J Biol Chem. 2012;287(3):1970–9.

Greenberg AS, Avila D, Hughes M, Hughes A, McKinney EC, Flajnik MF. A new antigen receptor gene family that undergoes rearrangement and extensive somatic diversification in sharks. Nature. 1995;374(6518):168–73.

Gulati S, Jin H, Masuho I, Orban T, Cai Y, Pardon E, Martemyanov KA, Kiser PD, Stewart PL, Ford CP, Steyaert J, Palczewski K. Targeting G protein-coupled receptor signaling at the G protein level with a selective nanobody inhibitor. Nat Commun. 2018;9(1):1996.

Hamers-Casterman C, Atarhouch T, Muyldermans S, Robinson G, Hammers C, Songa EB, Bendahman N, Hammers R. Naturally occurring antibodies devoid of light chains. Nature. 1993;363(6428):446–8.

Haskó G, Cronstein B. Regulation of Inflammation by Adenosine. Front Immunol. 2013;4.

Hussack G, Hirama T, Ding W, MacKenzie R, Tanha J. Engineered Single-Domain Antibodies with High Protease Resistance and Thermal Stability. PLOS ONE. 2011;6(11):e28218.

Idzko M, Ferrari D, Eltzschig HK. Nucleotide signalling during inflammation. Nature. 2014;509(7500):310–7.

Jacobson KA, Balasubramanian R, Deflorian F, Gao Z-G. G protein-coupled adenosine (P1) and P2Y receptors: ligand design and receptor interactions. Purinergic Signal. 2012;8(3):419–36.

Jank L, Pinto Espinoza C, Duan Y, Koch-Nolte F, Magnus T, Rissiek B. Current Approaches and Future Perspectives for Nanobodies in Stroke Diagnostic and Therapy. Antibodies. 2019;8:5.

Jeffrey JL, Lawson KV, Powers JP. Targeting Metabolism of Extracellular Nucleotides via Inhibition of Ectonucleotidases CD73 and CD39. J Med Chem. American Chemical Society; 2020;63(22):13444–65.

Jovčevska I, Muyldermans S. The Therapeutic Potential of Nanobodies. BioDrugs. 2020;34(1):11–26.

Kehoe JW, Kay BK. Filamentous Phage Display in the New Millennium. Chem Rev. 2005;105(11):4056–72.

Klämbt V, Wohlfeil SA, Schwab L, Hülsdünker J, Ayata K, Apostolova P, Schmitt-Graeff A, Dierbach H, Prinz G, Follo M, Prinz M, Idzko M, Zeiser R. A Novel Function for P2Y2 in Myeloid Recipient–Derived Cells during Graft-versus-Host Disease. J Immunol. 2015;195(12):5795–804.

Knowles AF. The GDA1_CD39 superfamily: NTPDases with diverse functions. Purinergic Signal. 2011;7(1):21–45.

Könning D, Zielonka S, Grzeschik J, Empting M, Valldorf B, Krah S, Schröter C, Sellmann C, Hock B, Kolmar H. Camelid and shark single domain antibodies: structural features and therapeutic potential. Curr Opin Struct Biol. 2017;45:10–6.

Li J-W, Xia L, Su Y, Liu H, Xia X, Lu Q, Yang C, Reheman K. Molecular Imprint of Enzyme Active Site by Camel Nanobodies: RAPID AND EFFICIENT APPROACH TO PRODUCE ABZYMES WITH ALLIINASE ACTIVITY *. J Biol Chem. Elsevier; 2012;287(17):13713–21.

Liu M, Li L, Jin D, Liu Y. Nanobody—A versatile tool for cancer diagnosis and therapeutics. WIREs Nanomedicine Nanobiotechnology. 2021;13(4):e1697.

Lommatzsch M, Cicko S, Müller T, Lucattelli M, Bratke K, Stoll P, Grimm M, Dürk T, Zissel G, Ferrari D, Di Virgilio F, Sorichter S, Lungarella G, Virchow JC, Idzko M. Extracellular adenosine triphosphate and chronic obstructive pulmonary disease. Am J Respir Crit Care Med. 2010;181(9):928–34.

Longhi MS, Moss A, Jiang ZG, Robson SC. Purinergic signaling during intestinal inflammation. J Mol Med. 2017;95(9):915–25.

Mai-Prochnow A, Hui JGK, Kjelleberg S, Rakonjac J, McDougald D, Rice SA. 'Big things in small packages: the genetics of filamentous phage and effects on fitness of their host.' FEMS Microbiol Rev. 2015;39(4):465–87.

McCafferty J, Griffiths AD, Winter G, Chiswell DJ. Phage antibodies: filamentous phage displaying antibody variable domains. Nature. 1990;348(6301):552–4.

Menegollo M, Tessari I, Bubacco L, Szabadkai G. Determination of ATP, ADP, and AMP Levels by Reversed-Phase High-Performance Liquid Chromatography in Cultured Cells. Methods Mol Biol Clifton NJ. 2019;1925:223–32.

Menzel S, Schwarz N, Haag F, Koch-Nolte F. Nanobody-Based Biologics for Modulating Purinergic Signaling in Inflammation and Immunity. Front Pharmacol. Frontiers; 2018;0.

Mitchell LS, Colwell LJ. Analysis of nanobody paratopes reveals greater diversity than classical antibodies. Protein Eng Des Sel. 2018a;31(7–8):267–75.

Mitchell LS, Colwell LJ. Comparative analysis of nanobody sequence and structure data. Proteins. 2018b;86(7):697–706.

Moesta AK, Li X-Y, Smyth MJ. Targeting CD39 in cancer. Nat Rev Immunol. 2020;20(12):739–55.

Mondal S, Hsiao K, Goueli SA. Utility of Adenosine Monophosphate Detection System for Monitoring the Activities of Diverse Enzyme Reactions. ASSAY Drug Dev Technol. Mary Ann Liebert, Inc., publishers; 2017;15(7):330–41.

Müller T, Fay S, Vieira RP, Karmouty-Quintana H, Cicko S, Ayata K, Zissel G, Goldmann T, Lungarella G, Ferrari D, Di Virgilio F, Robaye B, Boeynaems J-M, Blackburn MR, Idzko M. The purinergic receptor subtype P2Y2 mediates chemotaxis of neutrophils and fibroblasts in fibrotic lung disease. Oncotarget. 2017;8(22):35962–72.

Muyldermans S. Nanobodies: Natural Single-Domain Antibodies. Annu Rev Biochem. 2013;82(1):775–97.

Muyldermans S. A guide to: generation and design of nanobodies. FEBS J.

2021;288(7):2084–102.

Muyldermans S, Atarhouch T, Saldanha J, Barbosa JA, Hamers R. Sequence and structure of VH domain from naturally occurring camel heavy chain immunoglobulins lacking light chains. Protein Eng. 1994;7(9):1129–35.

Nikolova M, Carriere M, Jenabian M-A, Limou S, Younas M, Kök A, Huë S, Seddiki N, Hulin A, Delaneau O, Schuitemaker H, Herbeck JT, Mullins JI, Muhtarova M, Bensussan A, Zagury J-F, Lelievre J-D, Lévy Y. CD39/Adenosine Pathway Is Involved in AIDS Progression. PLoS Pathog. 2011;7(7).

Overman MJ, LoRusso P, Strickler JH, Patel SP, Clarke SJ, Noonan AM, Prasanna T, Amin MA, Nemunaitis JJ, Desai J, O'Byrne KJ, George TJ, Englert J, She D, Cooper ZA, Wu Y, Khan A, Kumar R, Bendell JC. Safety, efficacy and pharmacodynamics (PD) of MEDI9447 (oleclumab) alone or in combination with durvalumab in advanced colorectal cancer (CRC) or pancreatic cancer (panc). J Clin Oncol. 2018;36(15_suppl):4123–4123.

Parmley SF, Smith GP. Antibody-selectable filamentous fd phage vectors: affinity purification of target genes. Gene. 1988;73(2):305–18.

Rakonjac J, Bennett NJ, Spagnuolo J, Gagic D, Russel M. Filamentous bacteriophage: biology, phage display and nanotechnology applications. Curr Issues Mol Biol. 2011;13(2):51–76.

Ralevic V, Burnstock G. Receptors for Purines and Pyrimidines. Pharmacol Rev. 1998;50(3):413–92.

Rennhack JP, To B, Swiatnicki M, Dulak C, Ogrodzinski MP, Zhang Y, Li C, Bylett E, Ross C, Szczepanek K, Hanrahan W, Jayatissa M, Lunt SY, Hunter K, Andrechek ER. Integrated analyses of murine breast cancer models reveal critical parallels with human disease. Nat Commun. 2019;10(1):3261.

Roberts V, Lu B, Rajakumar S, Cowan PJ, Dwyer KM. The CD39-adenosinergic axis in the pathogenesis of renal ischemia–reperfusion injury. Purinergic Signal. 2013;9(2):135–43.

Robson SC, Sévigny J, Zimmermann H. The E-NTPDase family of ectonucleotidases: Structure function relationships and pathophysiological significance. Purinergic Signal. 2006;2(2):409–30.

Ruiz-Masó JA, MachóN C, Bordanaba-Ruiseco L, Espinosa M, Coll M, Del Solar G. Plasmid Rolling-Circle Replication. Microbiol Spectr. American Society for Microbiology; 2015;3(1):3.1.16.

Savio LEB, de Andrade Mello P, da Silva CG, Coutinho-Silva R. The P2X7 Receptor in Inflammatory Diseases: Angel or Demon? Front Pharmacol. 2018;9.

Schoonaert L, Rué L, Roucourt B, Timmers M, Little S, Chávez-Gutiérrez L, Dewilde M, Joyce P, Curnock A, Weber P, Haustraete J, Hassanzadeh-Ghassabeh G, Strooper BD, Bosch LVD, Damme PV, Lemmens R, Robberecht W. Identification and characterization of Nanobodies targeting the EphA4 receptor. J Biol Chem. Elsevier; 2017;292(27):11452–65.

Schroeder HW, Cavacini L. Structure and Function of Immunoglobulins. J Allergy Clin Immunol. 2010;125(2 0 2):S41–52.

Schrörs B, Boegel S, Albrecht C, Bukur T, Bukur V, Holtsträter C, Ritzel C,

Manninen K, Tadmor AD, Vormehr M, Sahin U, Löwer M. Multi-Omics Characterization of the 4T1 Murine Mammary Gland Tumor Model. Front Oncol. 2020;10:1195.

Schumacher D, Helma J, Schneider AFL, Leonhardt H, Hackenberger CPR. Nanobodies: Chemical Functionalization Strategies and Intracellular Applications. Angew Chem Int Ed. 2018;57(9):2314–33.

Scott AM, Wolchok JD, Old LJ. Antibody therapy of cancer. Nat Rev Cancer. 2012;12(4):278–87.

Shieh C-H, Heinrich A, Serchov T, Calker D van, Biber K. P2X7-dependent, but differentially regulated release of IL-6, CCL2, and TNF-α in cultured mouse microglia. Glia. 2014;62(4):592–607.

Simmons ZR, Sharma S, Wayne J, Li S, Kooi CWV, Gentry MS. Generation and characterization of a laforin nanobody inhibitor. bioRxiv. Cold Spring Harbor Laboratory; 2021;2021.01.20.426524.

Smith GP. Filamentous fusion phage: novel expression vectors that display cloned antigens on the virion surface. Science. 1985;228(4705):1315–7.

Spatola B, Lerner A, Wong C, Cruz T, Welch M, Fung W, Kovalenko M, Losenkova K, Yegutkin G, Beers C, Corbin J, Soros V. Fully human anti-CD39 antibody potently inhibits ATPase activity in cancer cells via uncompetitive allosteric mechanism. mAbs. 2020;12:e1838036.

Strausberg RL, Feingold EA, Grouse LH, Derge JG, Klausner RD, Collins FS, Wagner L, Shenmen CM, Schuler GD, Altschul SF, Zeeberg B, Buetow KH, Schaefer CF, Bhat NK, Hopkins RF, Jordan H, Moore T, Max SI, Wang J, Hsieh F, Diatchenko L, Marusina K, Farmer AA, Rubin GM, Hong L, Stapleton M, Soares MB, Bonaldo MF, Casavant TL, Scheetz TE, Brownstein MJ, Usdin TB, Toshiyuki S, Carninci P, Prange C, Raha SS, Loquellano NA, Peters GJ, Abramson RD, Mullahy SJ, Bosak SA, McEwan PJ, McKernan KJ, Malek JA, Gunaratne PH, Richards S, Worley KC, Hale S, Garcia AM, Gay LJ, Hulyk SW, Villalon DK, Muzny DM, Sodergren EJ, Lu X, Gibbs RA, Fahey J, Helton E, Ketteman M, Madan A, Rodrigues S, Sanchez A, Whiting M, Madan A, Young AC, Shevchenko Y, Bouffard GG, Blakesley RW, Touchman JW, Green ED, Dickson MC, Rodriguez AC, Grimwood J, Schmutz J, Myers RM, Butterfield YSN, Krzywinski MI, Skalska U, Smailus DE, Schnerch A, Schein JE, Jones SJM, Marra MA, Mammalian Gene Collection Program Team. Generation and initial analysis of more than 15,000 full-length human and mouse cDNA sequences. Proc Natl Acad Sci U S A. 2002;99(26):16899–903.

Sun X, Wu Y, Gao W, Enjyoji K, Csizmadia E, Müller CE, Murakami T, Robson SC. CD39/ENTPD1 Expression by CD4+Foxp3+ Regulatory T Cells Promotes Hepatic Metastatic Tumor Growth in Mice. Gastroenterology. 2010;139(3):1030–40.

Tang J, Pearce L, O'Donnell-Tormey J, Hubbard-Lucey VM. Trends in the global immuno-oncology landscape. Nat Rev Drug Discov. 2018;17(11):783–4.

Vu KB, Ghahroudi MA, Wyns L, Muyldermans S. Comparison of llama VH sequences from conventional and heavy chain antibodies. Mol Immunol. 1997;34(16):1121–31.

Wang L-L, Tang H-P, Shi G-C, Wan H-Y, Tang W, Hou X-X, Pan L-N, Shi B-Y, Tao L-Q. CD39/CD73 and the imbalance of Th17 cells and regulatory T cells in allergic asthma. Mol Med Rep. Spandidos Publications; 2013;8(5):1432–8.

Wesolowski J, Alzogaray V, Reyelt J, Unger M, Juarez K, Urrutia M, Cauerhff A, Danquah W, Rissiek B, Scheuplein F, Schwarz N, Adriouch S, Boyer O, Seman M, Licea A, Serreze DV, Goldbaum FA, Haag F, Koch-Nolte F. Single domain antibodies: promising experimental and therapeutic tools in infection and immunity. Med Microbiol Immunol (Berl). 2009;198(3):157–74.

Winter G, Griffiths AD, Hawkins RE, Hoogenboom HR. Making Antibodies by Phage Display Technology. Annu Rev Immunol. 1994;12(1):433–55.

Zavrtanik U, Lukan J, Loris R, Lah J, Hadži S. Structural Basis of Epitope Recognition by Heavy-Chain Camelid Antibodies. J Mol Biol. 2018;430(21):4369–86.

The Nobel Prize in Chemistry 2018. NobelPrize.org. 2018.

10. Lebenslauf

Personal Information:

Name: Yinghui Duan

Date of birth: 1990.04.20

Nationality: Chinese

Email: juliduan@163.com

Education:

2016 - 2021: Pursue the MD degree at University Medical Center Hamburg Eppendorf, Hamburg, Germany

2013 - 2016: Master of Neurology, Southeast University, China

2008 - 2013: Bachelor of Clinical Medicine, Southeast University, China

Awards and Honors:

Scholarship from China Scholarship Council (2016);

Excellent Resident Physician, Zhongda Hospital Affiliated Southeast University (2015)

Merit Graduate Student, Southeast University (2014);

Excellent Intern, Southeast University (2013);

National Scholarship, Ministry of Education of the People's Republic of China (2011 and 2015);

Donggang Dalian Scholarship, Southeast University (2011);

Model Student of Academic Records, Southeast University (2010);

Merit Student, Southeast University (2009 and 2011);

Academic Experience:

2020.11 2nd Retreat of the SFB1328 (online), Hamburg, Germany

2019.09 1st Bonn Nanobody Symptosium, Bonn, Germany

2019.03 1st Retreat of the SFB1328, Jesteburg, Germany

2013 - 2016: Standardized Resident Training in Zhongda Hospital, Southeast University, Nanjing, Jiangsu, China

2012 - 2013: Internship in the Third People's Hospital, Southeast University, Bengbu, Anhui, China

11. Acknowledgement

I sincerely thank my supervisor Tim Magnus for giving me the opportunity to join such a great research group and learn basic and advanced techniques, especially for providing me such a nice project and supporting me during the project undergoing. I am also very grateful for Björn Rissiek, who was always there whenever I met problems, gave me constructive suggestions and explained experiment designs and results patiently. Their passion on science are excellent models for me to keep curiosity on research.

Next, I would like to thank Stephan Menzel for giving me advice and explaining the theory about my project, especially on phage display. I also would like to thank Friedrich Koch-Nolte, Thomas Eden, Enja Schneider and Birte Albrecht for helping me on the material and technique support. I am thankful for Riekje Winzer. She kindly helped me on HPLC experiment, which is very important for the project completion.

Importantly, I appreciate the support from AG Magnus. They are wonderful colleagues helping me on techniques and supporting me whenever I needed help and support. The appreciation especially goes to Sarah Behr, for her kindly encourage and inspiration whenever I felt disappointment and support on techniques.

I would like to thank my family. Thanks to my parents, Jianshe Duan and Yinhua Si, owing to their understanding and support, I was able to pursue my dream reassuringly. In addition, I thank my brother and sister and my lovely nephew and nieces for their encouragement and love.

Last but not least, I'd like to thank the China Scholar Council, with their support I can be in such a beautiful city, Hamburg, and can complete my study without worries behind.

12. Eidesstattliche Versicherung

Ich versichere ausdrücklich, dass ich die Arbeit selbständig und ohne fremde Hilfe verfasst, andere als die von mir angegebenen Quellen und Hilfsmittel nicht benutzt und die aus den benutzten Werken wörtlich oder inhaltlich entnommenen Stellen einzeln nach Ausgabe (Auflage und Jahr des Erscheinens), Band und Seite des benutzten Werkes kenntlich gemacht habe.

Ferner versichere ich, dass ich die Dissertation bisher nicht einem Fachvertreter an einer anderen Hochschule zur Überprüfung vorgelegt oder mich anderweitig um Zulassung zur Promotion beworben habe.

Ich erkläre mich einverstanden, dass meine Dissertation vom Dekanat der Medizinischen Fakultät mit einer gängigen Software zur Erkennung von Plagiaten überprüft werden kann.

Unterschrift: .....